November 2006 were retrieved from the National Center for Biotechnology Information Refseq database. Very large multiple sequence alignments were constructed using MUSCLE 3.6 (Edgar 2004) and then 50 bacteria were chosen (supplementary table S2, Supplementary Material online) based on the alignments to retain at least a single species for each bacterial phylum and to eliminate species with organism-specific indels when possible. Amino acid sequences for 8 eukaryotes were deduced based on the sequenced genome databases (supplementary table S3, Supplementary Material online). Data matrices were constructed as follows: structure-based alignments were created for bacterial sequences using the Expresso (Armougom et al. 2006) Web service (http://www.tcoffee.org/), then eukaryotic sequences were added using ClustalX 1.83 (Thompson et al. 1997), and the results were manually refined and sites chosen for analysis. Although the Expresso Web service was used, ispG and ispH alignments were constructed by conventional methods because no suitable structural data were available for these genes. First, maximum likelihood (ML) trees were inferred with a WAG substitution matrix (Whelan and Goldman 2001) using Phyml 2.4.4 (Guindon and Gascuel 2003) with bootstrap values (100 replications), and distant problematic bacterial sequences (underlined in supplementary table S2, Supplementary Material online) were eliminated. Final ML trees were then inferred within additional operational taxonomic units (OTUs) for dinoflagellates and haptophytes, which have been obtained and synthesized from expressed sequence tags (EST) (source organisms and the original accession numbers are shown in the supplementary table S3, Supplementary Material online). Apicomplexan orthologs were excluded because they contain a vast number of changed or inserted residues, making it difficult to robustly infer phylogeny. In fact, trees drawn to include them resulted in placing them at deeper branches, disturbing tree topology, or reducing statistical support to greater or lesser degrees (data not shown).

Targeting Presequence Analysis

The N-terminal extensions of the translated amino acid sequences for each MEP pathway gene were examined using SignalP-HMM (Nielsen and Krogh 1998; Bendtsen et al. 2004) for SP and SOSUI (Hirokawa et al. 1998) for the transmembrane region. The distribution of protein sorting signals was examined using newly developed sliding-window iteration of TargetP (SWIT) analysis. Amino acid sequences were inferred from the first in-frame start codon, and subcellular localization was predicted by submitting the first 130 residues to the TargetP server (http://www.cbs.dtu.dk/services/TargetP/) (Nielsen et al. 1997; Emanuelsson et al. 2000); this was then repeated successively after eliminating the first residue from the N-terminus of the previously analyzed amino acid sequence (i.e., sliding a 130-residue window with a 1-residue step). Iterations were performed using the newly developed Ruby script, facilitated by the BioRuby library (http://www.bioruby.org/) (Goto et al. 2003). TargetP yields scores for SP, mitochondrial TP (mTP), chroloplast TP (cTP), and an other category for each iteration. The 4 scores were plotted with window positions on the y and x axes. Two superoxide dismutase genes, PmSOD1 and PmSOD2 (AY095212 and AY095213, respectively), were used for comparison (Wright et al. 2002).

Antibody

Rabbits were immunized with 2 synthesized peptides, TATVEDALKHPNWS and YTLAYPQRLHHDGS, which were partial fragments of the deduced ispC peptide sequence. A fraction of IgG (270 μg/ml) from the sera was obtained by affinity purification using the peptide cocktail to capture specific antibody. Recombinant ispC protein (with an N-terminal 6×His tag) lacking the predicted bipartite targeting peptide was expressed in *Escherichia coli* BL21-AI (Invitrogen) and was purified using HisTrap FF crude (GE Healthcare, Little Chalfont, Buckinghamshire, UK). We discovered that the cytosolic fraction of *P. marinus* contained a protein that nonspecifically reacted with normal rabbit IgG (Santa Cruz Biotechnology, Santa Cruz, CA); therefore, all antibodies were first adsorbed with proteins from the cytosolic fraction of *P. marinus* that were obtained by precipitation with 50–70% saturated ammonium sulfate.

Centrifugal Fractionation

Cells were collected by centrifugation (200 × g for 5 min at ambient temperature), washed with phosphate-buffered saline (PBS), resuspended in 50 mM *N*-2-hydroxyethylpiperazine-*N*′-2-ethanesulfonic acid buffer (pH 7.4) supplemented with protease inhibitor cocktail (Complete; F. Hofmann-La Roche, Basel, Switzerland), and disrupted by sonication on ice. The homogenate was subjected to differential centrifugal fractionation at 4 °C and divided into 4 fractions: 200 × g sediment (5 min), 2,000 × g sediment (10 min), 20,000 × g sediment (15 min), and the supernatant. The 20,000 × g sediment was incubated for 30 min at 4 °C in buffer containing 0.5% Triton X-100 and was then centrifuged at 20,000 × g for 15 min. All fractions were subjected to western blotting performed according to the following protocol: proteins separated by sodium dodecyl sulfate–polyacrylamide gel electrophoresis (10% gel) were transferred to PVDF membrane (Immobilon-P; Millipore, Billerica, MA), membranes were blocked for 1 h in blocking buffer (3% bovine serum albumin and 0.05% Tween 20 in PBS), and primary antibody (1:1000 dilution of the affinity-purified antibody) was added for 1 h. Next, alkaline phosphatase-conjugated Goat Anti-Rabbit IgG (Fc) (Promega S3731) in blocking buffer (1:7500) was added for 1 h and then the blots were developed by addition of BCIP/NBT Color Development Substrate (Promega S3771).

Immunofluorescent Microscopy

Cells were incubated for 30 min in culture medium containing 200 nM CMXRos (MitoTracker Red; Invitrogen M7512), washed for 15 min, and then fixed for 30 min at

−20 °C with 4% (w/v) paraformaldehyde in 85% (v/v) methanol. Fixed cells were washed with PBS and then mounted on Matsunami adhesive silane–coated slides (Matsunami Glass Industries, Kishiwada, Japan) and air dried. The slides were blocked for 1 h with BlockAce (Dainippon Sumitomo Pharma, Osaka, Japan) containing 4 μg/ml normal goat IgG (Santa Cruz Biotechnology), labeled for 1 hr with a 1:1000 dilution of affinity-purified antibody, and then incubated for 1 h with 1:400 dilution of Alexa Fluor 488 Goat Anti-Rabbit IgG (H + L; Invitrogen A11008) in Can Get Signal immunostain Solution A (Toyobo, Osaka, Japan). After counterstaining with 1 μg/ml 4′,6-diamidino-2-phenylindole (DAPI), the slides were observed under an epifluorescence microscope (Olympus BX60) equipped with cooled digital color camera (Olympus DP70). For negative control experiments, the affinity-purified antibody was omitted or substituted with the same concentration of normal rabbit IgG.

Results

MEP Pathway Genes

We first searched for MEP pathway genes using a similarity search service at the *P. marinus* genome database of TIGR (http://www.tigr.org/tdb/e2k1/pmg/) using red alga, green alga, and apicomplexan homologs as queries for each gene (identifiers are shown in supplementary table S3, Supplementary Material online). Irrespective of species used as queries, all homologs resulted in the same significant hits: single contigs for *dxs*, *ispC*, *ispE*, and *ispF* and 2 contigs for *ispG* and *ispH*. For the latter genes, the hits were located at the termini of contigs and were assumed to be single genes astride contig gaps. Thus, all these genes were thought to exist only in single copy. In contrast, MVA pathway genes were not found when we searched for them in a similar fashion.

Six out of 7 MEP pathway genes (fig. 1) were then sequenced in their entirety using gene-specific primers designed based on the contig sequences. No homolog of the gene responsible for the third step, *ispD*, was found in the database, and an attempt to amplify the gene using degenerate primers failed. Untranslated regions were short, 19–45 and 15–97 nt for the 5′ and 3′ ends, respectively.

Evolutionary Origin and Relationships

To investigate the evolutionary origin of the sequenced MEP pathway genes, we performed phylogenetic analyses using PBEs and a wide range of bacteria. The dxs ortholog of *P. marinus* clusters with those of PBEs, and they form a clade with the alpha-proteobacterial counterparts with 100% bootstrap support, which is independent of cyanobacterial orthologs (fig. 2). The ispC orthologs of *P. marinus* and PBEs form a clade with the cyanobacterial orthologs with 100% bootstrap support (fig. 3). For the ispE tree, eukaryotic orthologs, including that of *P. marinus* and chlamydial counterparts, form a weakly supported (76%) clade (fig. 4). The ispF ortholog of *P. marinus* clusters with those of PBE with weak bootstrap support (58%), but the clade has failed to show a relationship with specific

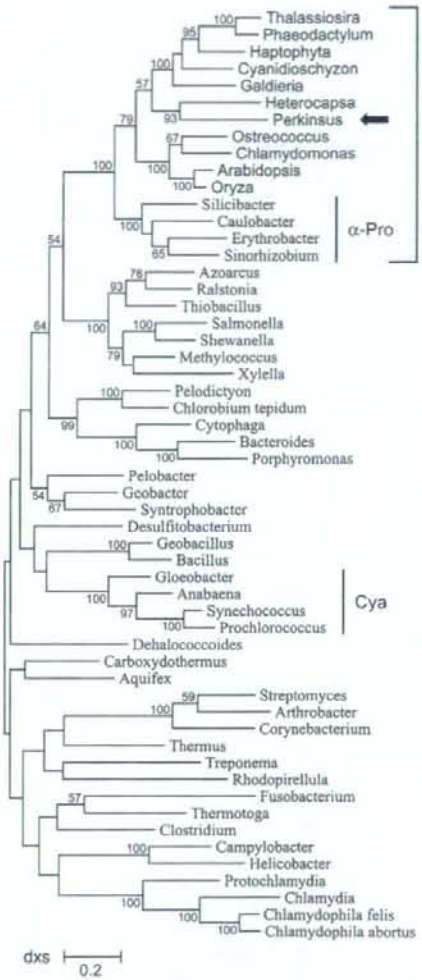

FIG. 2.—Unrooted ML tree for dxs (log likelihood= −35,861.100656) constructed using Phyml with WAG substitution matrix, based on a matrix comprising 55 OTUs and 497 sites. OTU names in sans serif indicate they are eukaryotic orthologs, and the bold arrow denotes the *Perkinsus marinus* ortholog. Haptophyta OTU is a synthetic sequence composed of *Emiliania*, *Isochrysis*, and *Pavlova* ESTs (supplementary table S3, Supplementary Material online) and lacks 23% of sites. Heterocapsa OTU is also a synthetic sequence derived from ESTs and lacks 6% of sites. Cyanobacterial (Cya) and alpha-proteobacterial (α-Pro) orthologs are indicated. Numbers adjacent to the nodes indicate bootstrap support (100 replicates), and values below 50% have been omitted. The scale bar indicates the number of substitutions per site.

bacteria (fig. 5). This is probably because of the shorter data matrix (104 sites), corroborated by poor phylogenetic resolution of the overall tree. For the ispG tree, the *P. marinus* ortholog and eukaryotic orthologs other than those from red algae form a clade with the chlamydial orthologs with 100% bootstrap support, whereas red algal orthologs form another clade with the cyanobacterial orthologs (fig. 6). The

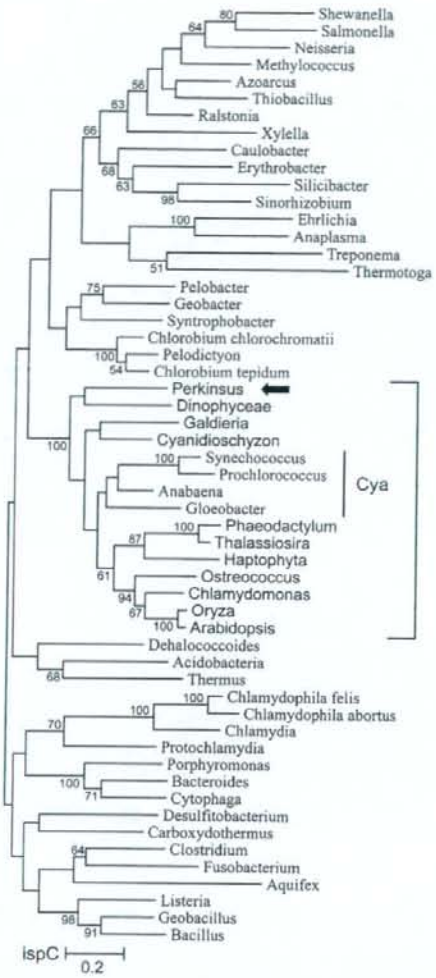

FIG. 3.—Unrooted ML tree for ispC (log likelihood = −25,588.615193) constructed using Phyml with WAG substitution matrix, based on a matrix comprising 55 OTUs and 337 sites. Haptophyta and Dinophyceae OTUs are synthetic sequences composed of *Emiliania* and *Isochrysis* ESTs, and *Alexandrium* and *Crypthecodinium* ESTs (supplementary table S3, Supplementary Material online), and lack 13% and 31% of sites, respectively. Cyanobacterial (Cya) orthologs are indicated. See also the legend of figure 2.

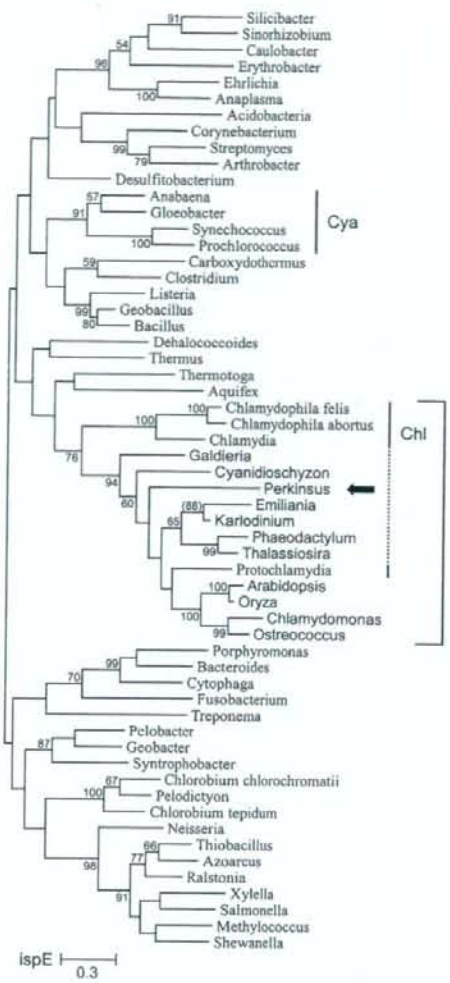

FIG. 4.—Unrooted ML tree for ispE (log likelihood = −16,236.630250) constructed using Phyml with WAG substitution matrix, based on a matrix comprising 58 OTUs and 175 sites. Emiliania and Karlodinium OTUs are partial sequences derived from ESTs (supplementary table S3, Supplementary Material online), lack 50% and 54% of sites, respectively, and do not overwrap; therefore, it could be an artifact that they form a clade although with a high bootstrap value (88, as indicated in parentheses). Cyanobacterial (Cya) and chlamydial (Chl) orthologs are indicated. See also the legend of figure 2.

ispH orthologs of *P. marinus* and PBEs form a clade with the cyanobacterial orthologs with 100% bootstrap support (fig. 7). All these results indicate that each of *P. marinus* orthologs clusters with the corresponding PBE orthologs; thus, the *P. marinus* orthologs are unlikely to have been independently transferred from bacteria.

Some of the *P. marinus* orthologs showed weak phylogenetic affinity to the dinoflagellate orthologs. The dxs ortholog formed a highly supported clade with the dinoflagellate *Heterocapsa* (fig. 2). The ispC ortholog formed a clade with a synthetic dinoflagellate OTU with <50% bootstrap support (fig. 3). Additionally, when a short sequence (105 sites) from the dinoflagellate *Amphidinium* ortholog was included in the ispG analysis, it was sister to the *Perkinsus* ortholog but with weak bootstrap support (54%). However, bootstrap supports for the adjacent nodes became weak, possibly due to the short dinoflagellate sequence (data not shown). The statistical weakness seems attributed to missing data derived from using partial ESTs of the dinoflagellate orthologs. In fact, the dxs tree, which has

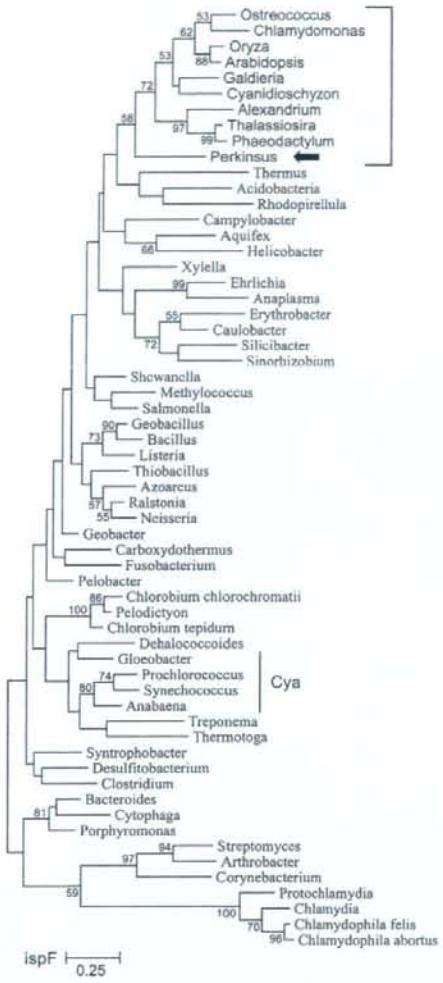

FIG. 5.—Unrooted ML tree for ispF (log likelihood = −7,405.683963) constructed using Phyml with WAG substitution matrix, based on a matrix comprising 60 OTUs and 104 sites. Alexandrium OTU is a partial sequence derived from ESTs (supplementary table S3, Supplementary Material online) and lacks 11% sites. Cyanobacterial (Cya) orthologs are indicated. See also the legend of figure 2.

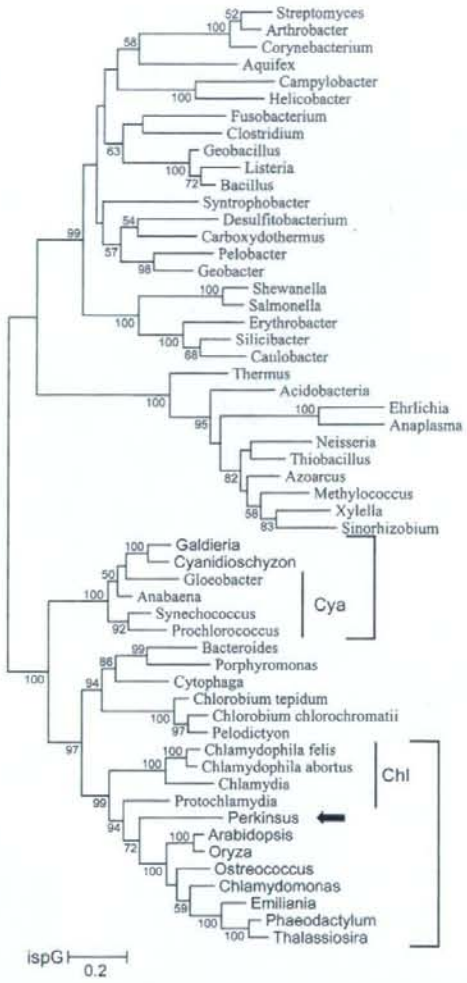

FIG. 6.—Unrooted ML tree for ispG (log likelihood = −21,369.78023) constructed using Phyml with WAG substitution matrix, based on a matrix comprising 55 OTUs and 344 sites. Emiliania OTU is a synthetic sequence derived from ESTs (supplementary table S3, Supplementary Material online). Amphidinium OTU was excluded because it was derived from a short EST and lacked 70% of sites; however, it was sister to the *Perkinsus* ortholog with weak (54%) bootstrap support when it was included in the matrix. Cyanobacterial (Cya) and chlamydial (Chl) orthologs are indicated. See also the legend of figure 2.

the strongest support, has the lowest amount of missing data (6% of sites) in the dinoflagellate ortholog. Therefore, the strength of this phylogenetic model may improve if full-length sequences become available. Reliable relationships for ispE and ispF orthologs of *P. marinus* were not resolved, and this was probably due to long-branch attraction or the shorter data matrix (figs. 4 and 5). The ispE tree (fig. 4) shows a highly supported close relationship between orthologs of the haptophyte *Emiliania* and the dinoflagellate *Karlodinium*. Although *Karlodinium* has a tertiary plastid derived from haptophytes, the close relationship should not be interpreted as a result of endosymbiotic gene transfer, but rather as an artifactual grouping of stray OTUs, because these 2 OTUs are derived from partial ESTs and have no overwrap on the sequence alignment. To summarize, in total, the MEP pathway genes of *P. marinus* have weak phylogenetic affinity to those of dinoflagellates, and this likely shows that the MEP pathway is descended from the common ancestor of *P. marinus* and dinoflagellates.

The present phylogenetic trees indicate that the MEP pathway genes of PBEs and *P. marinus* have essentially the

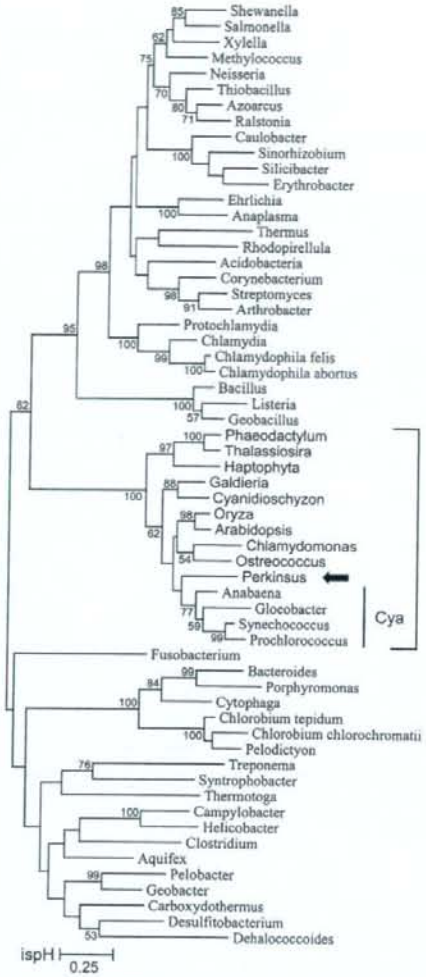

FIG. 7.—Unrooted ML tree for ispH (log likelihood = −18,623.672548) constructed using Phyml with WAG substitution matrix, based on a matrix comprising 60 OTUs and 230 sites. Haptophyta OTU is a synthetic sequence composed of *Emiliania* and *Pavlova* ESTs (supplementary table S3, Supplementary Material online) and lacks 10% of sites. Cyanobacterial (Cya) orthologs are indicated. See also the legend of figure 2.

same pattern of mosaic origins in Cyanobacteria, Proteobacteria, and Chlamydia (table 1). In PBEs, dxs (fig. 2) and ispE (fig. 4) had a sister relationship with the proteobacterial and chlamydial orthologs, respectively, whereas ispC and ispH seemed to be derived from Cyanobacteria (figs. 3 and 7). A chlamydial origin was also observed for ispD orthologs (supplementary fig. S1, Supplementary Material online). The evolutionary origin of ispF remains unclear, probably owing to insufficient informational sites being used (fig. 5). However, only red algae had cyanobacteria-like ispG orthologs, and *P. marinus* and other PBEs

Table 1
Shared Mosaic Origins of MEP Pathway Genes

	dxs	*ispC*	*ispD*	*ispE*	*ispF*	*ispG*	*ispH*
Green plants	pro	cya	chl	chl?	#	chl	cya
Red algae	pro	cya	chl	chl?	#	cya	cya
Diatoms	pro	cya	chl	chl?	#	chl	cya
Haptophytes	pro	cya	chl	chl?	—	chl	cya
Dinoflagellates	pro	cya	chl	chl?	#	chl?	—
Perkinsus	pro	cya	—	chl?	#	chl	cya

NOTE.—chl, chlamydia; cya, cyanobacteria; pro, α-proteobacteria; —, not found; ?, supported with weak bootstrap values; and #, monophyletic but showing no clear relationships.

harbored genes that were closely related to their chlamydial counterparts (fig. 6). This difference is not a phylogenetic artifact because there were long and well-aligned insertion sequences that were shared with PBEs other than red algae and Chlamydia (supplementary fig. S2, Supplementary Material online). The present phylogenetic analyses demonstrated that *P. marinus* and all PBEs analyzed here, with a curious exception of red algae, obtained their MEP pathway genes from an identical source.

Targeting Presequence and Subcellular Localization

The inferred amino acid sequences of the 6 MEP pathway genes in *P. marinus* have obvious N-terminal extensions relative to their bacterial homologs (fig. 1). N-terminal extensions often function as targeting presequences to deliver the peptide into certain subcellular compartments (e.g., ER, mitochondria, and plastids). First, SignalP predicted that all genes would have SPs (fig. 1; supplementary fig. S3, Supplementary Material online), although the probability of cleavage was not very high. Each predicted SP indicated an abnormally long (10–20 residues) hydrophilic n-region, but h- and c-regions were normal (supplementary fig. S3, Supplementary Material online). Because elimination of a few residues from the N-termini of the n-regions greatly improved the cleavage probability (data not shown), we consider that SPs with minor modification exist and they are likely cleaved off. The cleavable SP indicates that the MEP pathway enzymes are trafficked via the secretory pathway. However, TargetP predicted that all MEP pathway orthologs (except dxs) would be targeted to mitochondria. A lesson learned from the SignalP result is that simple predictions using full-length sequences may yield dubious results if the organism under question is distantly related to organisms after which the predictor has been modeled. Therefore, the need exists to monitor trends and the robustness of results obtained by TargetP analysis to better understand whether the mitochondrial targeting was significant and to further investigate the characteristics of the N-terminal extension.

We developed a new method of exploiting TargetP in order to robustly examine the distribution of targeting preferences. The method iteratively invoked TargetP with a sliding 130-residue window from the N-terminus; thus, we named the method SWIT. Figure 8 shows the SWIT results for the MEP pathway genes and 2 *P. marinus* superoxide dismutases, PmSOD1 and 2 (Wright et al. 2002). For

example, for dxs, a prediction with the first 130 residues yielded scores of 0.002, 0.062, 0.165, and 0.064 for cTP, mTP, SP, and others (*y* intercepts for green, blue, yellow, and gray lines), respectively; this is equivalent to the simple TargetP prediction using the full-length sequence. As the window slides downstream, the SP score increases up to 0.393 and then decreases to near zero. Although the first result (*y* intercept) alone, or the simple TargetP prediction, seems rather unreliable, we recognize that the N-terminal region likely has SP preference (yellow arrow). As the window slides along, a significant prominence for cTP appears (green arrow) in the vicinity of the predicted SP cleavage site (yellow triangle). The MEP pathway genes shared this characteristic SWIT trend, that is, a peak in the SP score at the N-terminal region and a subsequent increase in the cTP score. The trends seem to suggest that these enzymes are localized to secondary plastids because an N-terminal bipartite (SP + cTP) presequence is a characteristic feature of proteins of secondary plastids (van Dooren et al. 2001). Thus, we hypothetically considered residues between the N-terminus and the predicted SP cleavage site and between the SP cleavage site and the most downstream predicted site for cTP cleavage (green triangles) as putative SP and cTP, respectively.

One issue is that all aforementioned genes, except dxs, have considerable mTP scores at the *y* intercepts (fig. 8), which correspond to the simple TargetP results (see above). Both PmSOD1 and 2 also have high mTP scores at their N-termini, similar to the 5 MEP pathway genes (fig. 8); however, PmSOD2 localizes to an unknown, nonmitochondrial compartment, whereas PmSOD1 localizes to the mitochondria (Schott and Vasta 2003). According to the SWIT result, the mTP score for PmSOD1 is maintained along the N-terminal extension, and this corresponds to its mitochondrial localization; however, the score for PmSOD2 rapidly declines and SP and subsequent cTP preferences appear alternatively. Given that SP and cTP preferences do not appear for PmSOD1, they can be used to discriminate localization to a compartment other than the mitochondria; additionally, a high mTP score at the N-terminus has no biological significance when there are significant SP and cTP preferences. The MEP pathway genes share the SP + cTP feature with PmSOD2; thus, the MEP pathway genes appear to have protein sorting signals that are characteristic of proteins targeted to secondary plastids and to be localized to a compartment other than the mitochondria.

The predicted TP regions suggested by SWIT analysis were further examined in comparison to the TPs of PBEs. The predicted regions were overall hydrophilic and with a net positive charge, as in PBEs, resulting from depletion of acidic residues (5.3% compared with 12.9% in the homologous region) and accumulation of hydroxylated residues (especially Ser; 16.2% compared with 6.4%) and positive-charged residues (especially Arg; 7.1% compared with 5.2%). All but ispF were shown to possess Phe residues in a hydrophobic context in proximity to the SP cleavage site, and a single transmembrane helix followed by an Arg-rich region within the TP region (fig. 1; supplementary fig. S3, Supplementary Material online). This feature resembles a similar feature in the class I TP of peridinine dinoflagellates, and no apicomplexans reported so far harbor

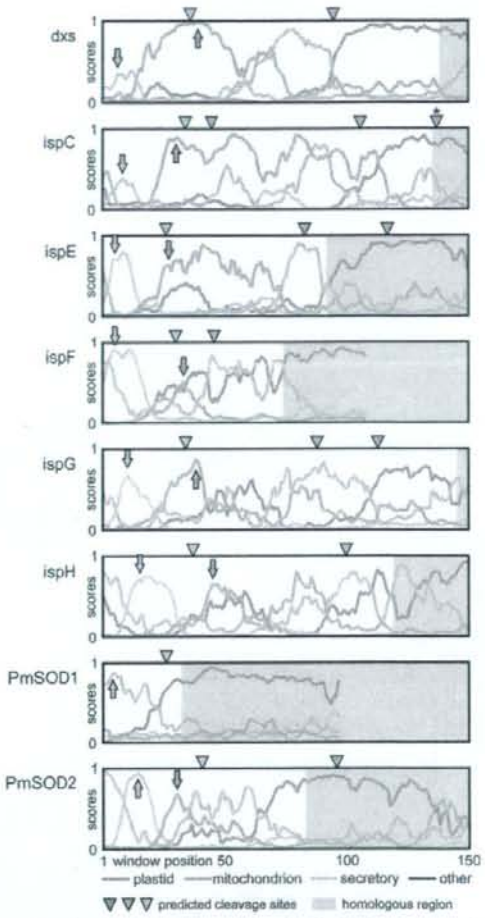

FIG. 8.—SWIT results showing the distribution of targeting preferences for the N-terminal presequences. For each gene, the neural network scores (*y* axis) of the TargetP prediction are plotted for the N-terminal 150 amino acids (*x* axis) in the following colors: green, plastid TP; light blue, mitochondrial TP; yellow, SP for secretory pathway; and gray, other location. Thus, the *y* intercepts correspond to the simple TargetP predictions. Triangles above each plot indicate the predicted cleavage sites: green, sites for plastid TP that appeared in the SWIT analysis; light blue, sites for mitochondrial TP (only for PmSOD1); and yellow, sites for SP as predicted by SignalP-HMM. The homologous region is shown in gray on each plot.

the transmembrane helix (Patron et al. 2005). No hydrophobic regions were predicted for ispF or PmSOD2, which makes them similar to the class II TP on the other hand (Patron et al. 2005). Collectively, the predicted TP regions resemble those of the peridinine dinoflagellates with respect to physicochemical features and class duality.

To examine whether the predicted bipartite targeting sequence is functional, a polyclonal antibody recognizing the second step enzyme coded by *ispC* was prepared. The affinity-purified antipeptide antibody successfully detected recombinant ispC (fig. 9*A*, lane 1), and it detected

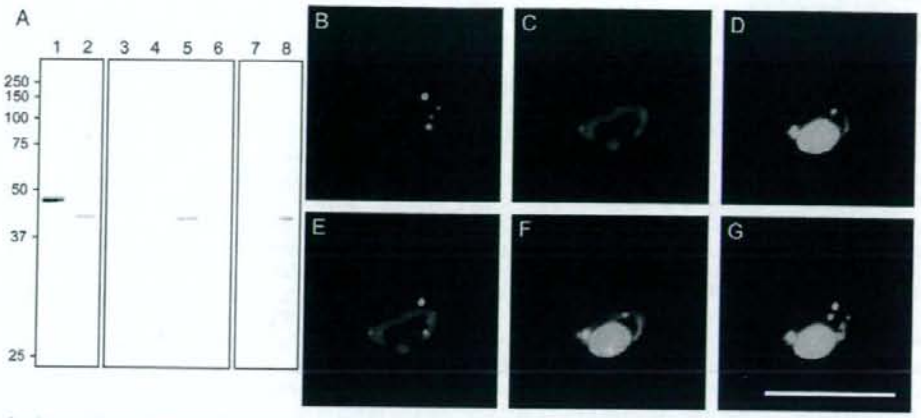

FIG. 9.—Immunological detection of the second step enzyme ispC. (*A*) Fractionation experiments for ispC. The size of ispC can be seen in lanes 1 and 2; a His-tagged recombinant ispC protein (1) acts as a positive control, and *Perkinsus marinus* cell lysate (2) contains native ispC. Lanes 3–6 show centrifugal fractionation of homogenized cell lysate; equivalent amounts of the 200 × g sediment (3), 2,000 × g sediment (4), 20,000 × g sediment (5), and 20,000 × g supernatant (6) were applied. Lanes 7 and 8 show the effect of Triton X-100 treatment on the 20,000 × g sediment (5); equivalent amounts of the 20,000 × g sediment (7) and 20,000 × g supernatant (8) were applied. Immunofluorescent microscopy indicating localization of ispC (*B–G*). Alexa Fluor 488 signals labeling ispC (*B*), CMXRos signals indicating mitochondria (*C*), and DAPI signals indicating DNA (*D*) were obtained from the same visual field. An overlaid image of ispC and mitochondria (*E*) indicates that the ispC protein localizes to punctate compartments near mitochondria. Those of DNA and mitochondria (*F*), and DNA and ispC (*G*) indicate that the mitochondria definitely contain DNA but the putative plastids do not contain detectable amounts of DNA. Bar indicates 10 μm.

a protein of approximately 43 kDa in *P. marinus* cell lysates (lane 2). Although smaller in size than predicted molecular weight of ispC (51 kDa), the size corresponds to an estimated molecular weight of the mature protein after cleavage of the predicted bipartite targeting peptides (asterisk in fig. 8). Detection at 43 kDa suggests that ispC is transported using targeting peptides that are subsequently cleaved. SOSUI predicted that the mature ispC protein was soluble. However, centrifugal fractionation showed the ispC protein specifically in the 20,000 × g sediment (lane 5), indicating that the protein was not cytosolic. The protein was easily solubilized by a mild detergent (lane 8), suggesting that it may be associated with membranes or membrane-bounded organelles. Finally, immunofluorescent microscopy revealed dotted signals for ispC (fig. 9*B*), and these signals were not associated with mitochondria (fig. 9*C*) or DNA (fig. 9*D*). Cells typically had multiple fluorescent spots that were frequently located near mitochondria (fig. 9*E*). Staining for extranuclear DNA overlapped with mitochondrial fluorescence (fig. 9*F*) but not with ispC fluorescence (fig. 9*G*).

Discussion

Plastids in *P. marinus*

The presence of 6 MEP pathway genes (fig. 1), together with the lack of any MVA pathway genes, suggests that the MEP pathway is responsible for de novo isoprenoid synthesis in *P. marinus*. A little possibility cannot be ruled out that the MEP pathway is not functional because we have been unable to find an *ispD* ortholog, but it does not impact on our logic for proving the existence of plastids in *P. marinus* (see below). Of course, activity of the MEP pathway still requires characterization in order to further discuss plastid function; however, this is beyond the scope of the present study.

The *P. marinus* genes reported here are very likely relevant to plastids because the MEP pathway is specific to PBE, all PBEs have obtained the genes from essentially the same source (table 1), and all MEP pathway genes of *P. marinus* consistently group with them (figs. 2–7). Furthermore, the fact that all these genes have the bipartite targeting sequence (figs. 1 and 8), plus the fact that the predicted targeting sequences are cleaved (fig. 9*A*, lane 2), supports our idea that these enzymes traffic using machinery homologous to those of secondary PBEs. Finally, a subcellular fractionation experiment indicated that ispC is not cytosolic and is associated with membranes or organelles (fig. 9*A*, lanes 5 and 8), and immunofluorescent microscopy showed punctate localization of ispC near mitochondria (fig. 9*E*). Generally said, if a group of proteins accumulates at a subcellular compartment by means of machinery reasonably homologous to that of plastids, that compartment should be identified as a plastid. Although recent studies have shown the evidence for *P. marinus* plastid (Stelter et al. 2007; Teles-Grilo et al. 2007), no direct evidence that completely fulfills this criterion has been presented. To our knowledge, we are the first to use proper evidence in order to demonstrate that *P. marinus* harbors secondary plastids.

We revealed the existence of *P. marinus* plastids by detecting ispC using immunofluorescent microscopy. However, our SWIT analysis showed that ispF and PmSOD2 had similar but slightly different bipartite presequences (figs. 1 and 8). Although PmSOD2 has also shown punctate localization (Schott and Vasta 2003), it remains to be elucidated whether ispC and PmSOD2 are colocalized. Another point to be examined is that the ispC spots do not

overwrap with DNA signals (fig. 9*G*). Given that staining of mitochondrial DNA is definitive (fig. 9*F*), the putative plastids seem to contain very low quantities of DNA or may even lack DNA. Our preliminary search of the TIGR genome database suggests that *P. marinus* has genes for mitochondrial DNA and RNA polymerases, elongation factors, and ribosomal proteins but seemingly lacks those for plastid counterparts (data not shown). There are no examples in the literature of DNA-lacking plastids; however, we know of many independent reports that show modified or degenerated mitochondria that lack DNA (Hackstein et al. 2006). It is thus worth considering the possibility of DNA-lacking plastids in *P. marinus*, although this remains to be confirmed experimentally.

We have shown the presence of secondary plastids in *P. marinus* by immunofluorescent microscopy; however, no corresponding structure has been found in EM specimens sampled from the same culture (Kuroiwa H, unpublished data). Upon conducting a literature review, we found that 3 candidate ultrastructures have been observed in allied organisms. One is a "coiled membrane system" near the mitochondria that was found in the oldest observations of *P. marinus* zoosporulation (Perkins and Menzel 1967). Although this structure has been considered a morphological variant of the mitochondria, it could also be interpreted as a multimembrane-bounded plastid resembling the apicoplast of the malarial parasite *Plasmodium falciparum* (Hopkins et al. 1999). Another candidate structure is the "enigmatic body" found in a related organism, *Rastrimonas subtilis* (Brugerolle 2002, 2003), which is limited by 2 or more membranes and is akin to the apicoplast of *Toxoplasma gondii* in spherical appearance and juxtanuclear localization (Matsuzaki et al. 2001; Köhler 2005); however, the assumed relationship between *R. subtilis* and *Perkinsus* spp. is based only on morphology and is currently unsupported by molecular information. Finally, a putative plastid bounded by 4 membranes was recently reported in *P. olseni* (=*P. atlanticus*) (Teles-Grilo et al. 2007). If this is the plastid to which the MEP pathway enzymes target, connection between the TP with a transmembrane helix and a plastid bounded by 3 membranes should be reconsidered. It is interesting that all 3 candidate structures have been observed in the respective organisms' flagellated stage and that no relevant structures have been reported at the EM level from nonflagellated cultures. Our results indicate that the nonflagellated cultures contain plastids (fig. 9*B*). It is possible that the plastid is in a degenerated form and is therefore overlooked in the nonflagellated stages at the EM level and develops during the course of differentiation into the flagellated stages. Note that ultrastructure alone (e.g., number of membranes) is inadequate to identify plastids (Köhler 2006); immunological labeling of the ultrastructure is required for confirmation, for which our affinity-purified antibody to ispC would be useful.

That the putative *P. marinus* plastid and the peridinine plastids share a common origin was suggested by the phylogenetic affinity between some MEP pathway genes and those of the peridinine dinoflagellates and the predicted features of the *P. marinus* TPs. The *P. marinus* TPs predict that the putative plastid is bounded by 3 membranes because TP with transmembrane helix seems to correspond to plastids with 3 bounding membranes, such as those found in dinoflagellates and euglenoids (Patron et al. 2005). Given that *Perkinsus* spp. are located basally to dinoflagellates (Cavalier-Smith and Chao 2004; Leander and Keeling 2004), it is reasonable to suppose that a common ancestor harbored a plastid that diverged to form the *P. marinus* and peridinine plastids. *Perkinsus marinus* has TPs that are reminiscent of those found in peridinine dinoflagellates (fig. 1), although unusual TPs have been found in dinoflagellates containing haptophyte-derived plastids (Patron et al. 2006); thus, the result supports the hypothesis that haptophyte-derived plastids are a derived feature (Yoon et al. 2005). Study of the MEP pathway genes in other nonphotosynthetic taxa of Dinozoa, such as *Oxyrrhis*, *Syndinium*, and *Noctiluca*, may reveal the presence of cryptic plastids. On the other hand, the *Perkinsus* MEP pathway genes failed to show a relationship with apicomplexan orthologs (data not shown) possibly because the apicomplexan OTUs were a strong source of a long-branch attraction artifact. The relationship between the putative plastid of *P. marinus* and the apicoplast is thus still open question. Because the nonphotosynthetic free-living flagellates, *Colpodella* spp., are phylogenetically basal to the apicomplexans (Kuvardina et al. 2002; Cavalier-Smith and Chao 2004; Skovgaard et al. 2005), investigating whether *Colpodella* contains plastids would be interesting. The putative plastid in *P. marinus* will be a key to verifying the chromalveolate hypothesis and will partially rebut its critics (Bodył 2005).

Implications for Plastid Evolution

Our phylogenetic analyses showed that the MEP pathway of PBEs has an apparently mosaic origin in Cyanobacteria, Proteobacteria, and Chlamydia (table 1). Although an earlier study with limited sampling gave similar results for 5 genes (dxs to ispF) (Lange et al. 2000), the present results reinforce the evolutionary origins by using a wide range of bacteria. We also showed that the mosaic pattern was essentially the same among PBEs, including *P. marinus*, as is often the case with other plastid-related mosaic pathways, such as the Calvin cycle, heme biosynthesis, and the shikimate pathway (Matsuzaki et al. 2004; Obornik and Green 2005; Richards et al. 2006). Thus, we assume that the mosaic pattern was established before radiation of a wide variety of plastids, again supporting a single origin for plastids (Bhattacharya et al. 2004; Matsuzaki et al. 2004). It is natural that the cyanobacterial genes would be introduced during the primary endosymbiotic event, but the contribution of chlamydial genes seems rather peculiar. The apparent affinity could be interpreted as an artifact of interbacterial gene replacement (Lange et al. 2000; Rujan and Martin 2001); however, we consider that the observed mosaic pattern reflects an actual contribution by Chlamydia, because Chlamydia-related higher plant genes are biased toward plastid functions (Brinkman et al. 2002), and the bias is difficult to explain without assuming a connection between Chlamydia and plastids.

The ispG alignment (supplementary fig. S2, Supplementary Material online) and phylogenetic tree (fig. 6) show that the origin of the red algal orthologs clearly differed from that of orthologs from other PBEs. This seems

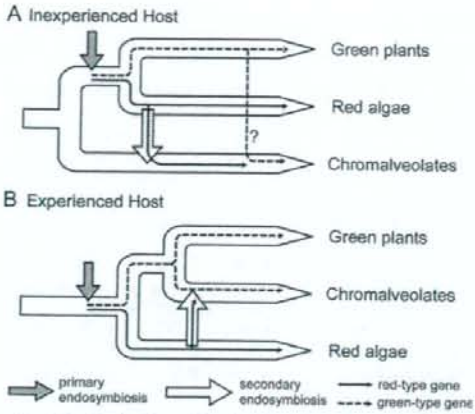

FIG. 10.—Explanation of the phylogenetic affinity to green plants in the cyanobacterial genes from chromalveolates, in 2 alternative phylogenetic trees of the host eukaryotes. (*A*) The inexperienced host model. If the ancestral chromalveolate host was inexperienced with primary plastids, red-type genes (solid arrows) must have been introduced and used in the chromalveolates at the secondary endosymbiotic event (unfilled arrow). Then, the green-type genes (broken arrows) may have been introduced via an unknown lateral gene transfer (LGT) event (indicated by "?") and replaced the red-type genes. (*B*) The experienced host model. Assuming that the ancestral host organism was experienced with primary plastids, 2 options exist for the secondary endosymbiotic event: retaining the green-type genes inherited from the ancestor or accepting the red-type genes transferred from the symbiont. In this case, the discrepancy can be explained without any further LGT event.

unusual, but other genes also show a similar difference between red algae and other PBEs, for example, enoyl acyl carrier protein reductase (Matsuzaki M, unpublished data) and plastid ferrochelatase (Oborník and Green 2005). This discrepancy in the phylogenetic positions of genes in red algae and the chromalveolates can be explained by the evolutionary histories of the symbiotic hosts (fig. 10). Two competing inferences exist for PBE phylogeny: the chromalveolates are independent of primary PBEs and are inexperienced with primary plastids (Rodríguez-Ezpeleta et al. 2005) (fig. 10*A*) and the chromalveolates originate from an in-group of primary PBEs and are experienced with primary plastids (Nozaki et al. 2003, 2007) (fig. 10*B*). Because it is widely accepted that the plastid progenitor in the chromalveolates is a kind of, or belongs to a sister group of, ancestral red algae (Fast et al. 2001; Yoon et al. 2002, 2005), the former topology predicts that red algae and the chromalveolates contain genes of the same cyanobacterial origin and requires extra loss, gain, or transfer events to explain the observed differences (fig. 10*A* shows a transfer event from the green plant lineage, which is the simplest). For the latter topology, the chromalveolates have 2 possible sources for plastid genes, the host ancestor and the symbiont. In this scenario, genes related to those of green plants can be inherited as constituents of the host genome and can be retained and used after the secondary endosymbiotic event. We prefer the latter model (fig. 10*B*) because it does not require additional transfer events other than the 2 widely accepted endosymbiotic events. In addition, this scenario can explain the frequently observed incoherence of the phylogenetic affinity of diatom genes, for example, the MEP pathway (figs. 2–7), the shikimate pathway (Richards et al. 2006), and the heme biosynthesis pathway (Oborník and Green 2005), in which the diatom ortholog for each gene has phylogenetic affinities to either green plants or red algae. Genes with an affinity to green plants and red algae could be derived from the host eukaryote and the plastid progenitor at the secondary symbiotic event, respectively. Furthermore, this scenario implies that the host eukaryote of the secondary endosymbiotic event that forms the chromalveolate ancestor must have retained the primary plastid originating from the ancient primary endosymbiosis because the MEP pathway seems to be specific to PBEs; then, it was replaced with the secondary plastid obtained from the engulfed red alga.

Conclusion

The existence of the plastid and its affinity to those of dinoflagellates, as suggested in the present study, greatly changes our view of *P. marinus*. It was first described as a pathogenic protist, then subsequently reclassified as a fungal or sporozoan species, and has recently been treated as an alveolate flagellate (Villalba et al. 2004; Adl et al. 2005); however, *P. marinus* is a cryptic alga in terms of plastid existence. Our identification of a *Perkinsus* spp. plastid will make this algal organism key in discussions of plastid evolution. Furthermore, just as discovery of the apicoplast has revolutionized malaria chemotherapy, the algal nature of *Perkinsus* spp. may permit novel approaches for controlling perkinsosis in fisheries.

Supplementary Material

Supplementary tables S1–S3 and figures S1–S3 are available at *Molecular Biology and Evolution* online (http://www.mbe.oxfordjournals.org/).

Acknowledgments

Preliminary sequence data for *P. marinus* were obtained from The Institute for Genomic Research via their Web site at http://www.tigr.org/. Sequencing of the *P. marinus* genome was accomplished with support from the US National Science Foundation. The genome sequence data for *Galdieria sulphuraria* were obtained from the Michigan State University Galdieria Database (http://genomics.msu.edu/galdieria/). The genome sequence data for *Chlamydomonas reinhardtii*, *Ostreococcus lucimarinus*, *Phaeodactylum tricornutum*, and *Thalassiosira pseudonana* were obtained from the US Department of Energy Joint Genome Institute (http://www.jgi.doe.gov/) and are provided for use in this publication only. The authors thank Dr Shin-ichiro Maruyama and Dr Takashi Nakada (the University of Tokyo) for helpful discussions and comments on figure presentation and Dr Shigeharu Sato (National Institute for Medical Research, UK) for providing valuable information on related topics. This study was supported by Grants-in-Aid

for Creative Scientific Research (16GS0304 to H.N. and 18GS0314 to K.K.), for Scientific Research (17370087 to H.N. and 18073004 for K.K.), and for the Japan Society for the Promotion of Science (JSPS) Fellows (17-10695 to M.M.) from the JSPS and the Ministry of Education, Culture, Sports, Science, and Technology (MEXT); by a matching fund subsidy for "Academic Frontier" Projects (to T.K.) from MEXT; and by the Program for the Promotion of Basic Research Activities for Innovative Biosciences (to T.K.). M.M. is a Research Fellow of the JSPS.

Literature Cited

Adl SM, Simpson AGB, Farmer MA, et al. (28 co-authors). 2005. The new higher level classification of eukaryotes with emphasis on the taxonomy of protists. J Eukaryot Microbiol. 52:399–451.

Armougom F, Moretti S, Poirot O, Audic S, Dumas P, Schaeli B, Keduas V, Notredame C. 2006. Expresso: automatic incorporation of structural information in multiple sequence alignments using 3D-Coffee. Nucleic Acids Res. 34:W604–W608.

Bendtsen JD, Nielsen H, von Heijne G, Brunak S. 2004. Improved prediction of signal peptides: signalP 3.0. J Mol Biol. 340:783–795.

Bhattacharya D, Yoon HS, Hackett JD. 2004. Photosynthetic eukaryotes unite: endosymbiosis connects the dots. Bioessays. 26:50–60.

Bodył A. 2005. Do plastid-related characters support the chromalveolate hypothesis? J Phycol. 41:712–719.

Brinkman FSL, Blanchard JL, Cherkasov A, et al. (14 co-authors). 2002. Evidence that plant-like genes in Chlamydia species reflect an ancestral relationship between Chlamydiaceae, cyanobacteria, and the chloroplast. Genome Res. 12:1159–1167.

Brugerolle G. 2002. *Cryptophagus subtilis*: a new parasite of cryptophytes affiliated with the Perkinsozoa lineage. Eur J Protistol. 37:379–390.

Brugerolle G. 2003. Apicomplexan parasite *Cryptophagus* renamed *Rastrimonas* gen. nov. Eur J Protistol. 39:101.

Cavalier-Smith T. 1999. Principles of protein and lipid targeting in secondary symbiogenesis: euglenoid, dinoflagellate, and sporozoan plastid origins and the eukaryote family tree. J Eukaryot Microbiol. 46:347–366.

Cavalier-Smith T, Chao EE. 2004. Protalveolate phylogeny and systematics and the origins of Sporozoa and dinoflagellates (phylum Myzozoa nom. nov.). Eur J Protistol. 40:185–212.

Derelle E, Ferraz C, Rombauts S, et al. (26 co-authors). 2006. Genome analysis of the smallest free-living eukaryote *Ostreococcus tauri* unveils many unique features. Proc Natl Acad Sci USA. 103:11647–11652.

Edgar RC. 2004. MUSCLE: multiple sequence alignment with high accuracy and high throughput. Nucleic Acids Res. 32:1792–1797.

Emanuelsson O, Nielsen H, Brunak S, von Heijne G. 2000. Predicting subcellular localization of proteins based on their N-terminal amino acid sequence. J Mol Biol. 300:1005–1016.

Fast NM, Kissinger JC, Roos DS, Keeling PJ. 2001. Nuclear-encoded, plastid-targeted genes suggest a single common origin for apicomplexan and dinoflagellate plastids. Mol Biol Evol. 18:418–426.

Gardner MJ, Bishop R, Shah T, et al. (44 co-authors). 2005. Genome sequence of *Theileria parva*, a bovine pathogen that transforms lymphocytes. Science. 309:134–137.

Gardner MJ, Hall N, Fung E, et al. (45 co-authors). 2002. Genome sequence of the human malaria parasite *Plasmodium falciparum*. Nature. 419:498–511.

Goto N, Nakao MC, Kawashima S. 2003. BioRuby: open-source bioinformatics library. Genome Inform. 14:629–630.

Guindon S, Gascuel O. 2003. A simple, fast, and accurate algorithm to estimate large phylogenies by maximum likelihood. Syst Biol. 52:696–704.

Hackstein JHP, Tjaden J, Huynen M. 2006. Mitochondria, hydrogenosomes and mitosomes: products of evolutionary tinkering! Curr Genet. 50:225–245.

Hirokawa T, Boon-Chieng S, Mitaku S. 1998. SOSUI: classification and secondary structure prediction system for membrane proteins. Bioinformatics. 14:378–379.

Hopkins J, Fowler R, Krishna S, Wilson I, Mitchell G, Bannister L. 1999. The plastid in *Plasmodium falciparum* asexual blood stages: a three-dimensional ultrastructural analysis. Protist. 150:283–295.

Köhler S. 2005. Multi-membrane-bound structures of Apicomplexa: I. the architecture of the *Toxoplasma gondii* apicoplast. Parasitol Res. 96:258–272.

Köhler S. 2006. Multi-membrane-bound structures of Apicomplexa: II. the ovoid mitochondrial cytoplasmic (OMC) complex of *Toxoplasma gondii* tachyzoites. Parasitol Res. 98: 355–369.

Kuvardina ON, Leander BS, Aleshin VV, Myl'nikov AP, Keeling PJ, Simdyanov TG. 2002. The phylogeny of colpodellids (Alveolata) using small subunit rRNA gene sequences suggests they are the free-living sister group to apicomplexans. J Eukaryot Microbiol. 49:498–504.

Lange BM, Rujan T, Martin W, Croteau R. 2000. Isoprenoid biosynthesis: the evolution of two ancient and distinct pathways across genomes. Proc Natl Acad Sci USA. 97:13172–13177.

Leander BS, Keeling PJ. 2004. Early evolutionary history of dinoflagellates and apicomplexans (Alveolata) as inferred from hsp90 and actin phylogenies. J Phycol. 40:341–350.

Matsuzaki M, Kikuchi T, Kita K, Kojima S, Kuroiwa T. 2001. Large amounts of apicoplast nucleoid DNA and its segregation in *Toxoplasma gondii*. Protoplasma. 218:180–191.

Matsuzaki M, Misumi O, Shin-i T, et al. (42 co-authors). 2004. Genome sequence of the ultrasmall unicellular red alga *Cyanidioschyzon merolae* 10D. Nature. 428:653–657.

Nielsen H, Engelbrecht J, Brunak S, von Heijne G. 1997. Identification of prokaryotic and eukaryotic signal peptides and prediction of their cleavage sites. Protein Eng. 10:1–6.

Nielsen H, Krogh A. 1998. Prediction of signal peptides and signal anchors by a hidden Markov model. Proc Int Conf Intell Syst Mol Biol. 6:122–130.

Not F, Valentin K, Romari K, Lovejoy C, Massana R, Töbe K, Vaulot D, Medlin LK. 2007. Picobiliphytes: a marine picoplanktonic algal group with unknown affinities to other eukaryotes. Science. 315:253–255.

Nozaki H, Iseki M, Hasegawa M, Misawa K, Nakada T, Sasaki N, Watanabe M. 2007. Phylogeny of primary photosynthetic eukaryotes as deduced from slowly evolving nuclear genes. Mol Biol Evol. 24:1592–1595.

Nozaki H, Matsuzaki M, Takahara M, Misumi O, Kuroiwa H, Hasegawa M, Shin-i T, Kohara Y, Ogasawara N, Kuroiwa T. 2003. The phylogenetic position of red algae revealed by multiple nuclear genes from mitochondria-containing eukaryotes and an alternative hypothesis on the origin of plastids. J Mol Evol. 56:485–497.

Oborník M, Green BR. 2005. Mosaic origin of the heme biosynthesis pathway in photosynthetic eukaryotes. Mol Biol Evol. 22:2343–2353.

Patron NJ, Waller RF, Archibald JM, Keeling PJ. 2005. Complex protein targeting to dinoflagellate plastids. J Mol Biol. 348: 1015–1024.

Patron NJ, Waller RF, Keeling PJ. 2006. A tertiary plastid uses genes from two endosymbionts. J Mol Biol. 357:1373–1382.

Perkins FO. 1976. Zoospores of the oyster pathogen, *Dermocystidium marinum*. I. Fine structure of the conoid and other sporozoan-like organelles. J Parasitol. 62:959–974.

Perkins FO. 1996. The structure of *Perkinsus marinus* (Mackin, Owen and Collier, 1950) Levine, 1978 with comments on taxonomy and phylogeny of Perkinsus spp. J Shellfish Res. 15:67–87.

Perkins FO, Menzel RW. 1967. Ultrastructure of sporulation in the oyster pathogen *Dermocystidium marinum*. J Invertebr Pathol. 9:205–229.

Richards TA, Dacks JB, Campbell SA, Blanchard JL, Foster PG, McLeod R, Roberts CW. 2006. Evolutionary origins of the eukaryotic shikimate pathway: gene fusions, horizontal gene transfer, and endosymbiotic replacements. Eukaryot Cell. 5:1517–1531.

Rodríguez-Concepción M. 2004. The MEP pathway: a new target for the development of herbicides, antibiotics and antimalarial drugs. Curr Pharm Des. 10:2391–2400.

Rodríguez-Ezpeleta N, Brinkmann H, Burey SC, Roure B, Burger G, Löffelhardt W, Bohnert HJ, Philippe H, Lang BF. 2005. Monophyly of primary photosynthetic eukaryotes: green plants, red algae, and glaucophytes. Curr Biol. 15:1325–1330.

Rujan T, Martin W. 2001. How many genes in Arabidopsis come from cyanobacteria? An estimate from 386 protein phylogenies. Trends Genet. 17:113–120.

Schott EJ, Vasta GR. 2003. The *PmSOD1* gene of the protistan parasite *Perkinsus marinus* complements the *sod2Δ* mutant of *Saccharomyces cerevisiae*, and directs an iron superoxide dismutase to mitochondria. Mol Biochem Parasitol. 126:81–92.

Skovgaard A, Massana R, Balagué V, Saiz E. 2005. Phylogenetic position of the copepod-infesting parasite *Syndinium turbo* (Dinoflagellata, Syndinea). Protist. 156:413–423.

Stelter K, El-Sayed NM, Seeber F. 2007. The expression of a plant-type ferredoxin redox system provides molecular evidence for a plastid in the early dinoflagellate *Perkinsus marinus*. Protist. 158:119–130.

Sunila I, Hamilton RM, Dungan CF. 2001. Ultrastructural characteristics of the in vitro cell cycle of the protozoan pathogen of oysters, *Perkinsus marinus*. J Eukaryot Microbiol. 48:348–361.

Teles-Grilo ML, Tato-Costa J, Duarte SM, Maia A, Casal G, Azevedo C. 2007. Is there a plastid in *Perkinsus atlanticus* (Phylum Perkinsozoa)? Eur J Protistol. 43:163–167.

Thompson JD, Gibson TJ, Plewniak F, Jeanmougin F, Higgins DG. 1997. The CLUSTAL_X windows interface: flexible strategies for multiple sequence alignment aided by quality analysis tools. Nucleic Acids Res. 25:4876–4882.

van Dooren GG, Schwartzbach SD, Osafune T, McFadden GI. 2001. Translocation of proteins across the multiple membranes of complex plastids. Biochim Biophys Acta. 1541: 34–53.

Villalba A, Reece KS, Ordás MC, Casas SM, Figueras A. 2004. Perkinsosis in molluscs: a review. Aquat Living Resour. 17:411–432.

Whelan S, Goldman N. 2001. A general empirical model of protein evolution derived from multiple protein families using a maximum-likelihood approach. Mol Biol Evol. 18:691–699.

Wilson RJM. 2005. Parasite plastids: approaching the endgame. Biol Rev Camb Philos Soc. 80:129–153.

Wright AC, Ahmed H, Gauthier JD, Silva AM, Vasta GR. 2002. cDNA cloning and characterization of two iron superoxide dismutases from the oyster parasite *Perkinsus marinus*. Mol Biochem Parasitol. 123:73–77.

Yoon HS, Hackett JD, Pinto G, Bhattacharya D. 2002. The single, ancient origin of chromist plastids. Proc Natl Acad Sci USA. 99:15507–15512.

Yoon HS, Hackett JD, Van Dolah FM, Nosenko T, Lidie KL, Bhattacharya D. 2005. Tertiary endosymbiosis driven genome evolution in dinoflagellate algae. Mol Biol Evol. 22: 1299–1308.

Takashi Gojobori, Associate Editor

Accepted March 14, 2008

Current Biology 18, 607–613, April 22, 2008 ©2008 Elsevier Ltd All rights reserved DOI 10.1016/j.cub.2008.03.045

Report

Male Fertility of Malaria Parasites Is Determined by GCS1, a Plant-Type Reproduction Factor

Makoto Hirai,[1,8,*] Meiji Arai,[2,8] Toshiyuki Mori,[3,8] Shin-ya Miyagishima,[3] Satoru Kawai,[4] Kiyoshi Kita,[5] Tsuneyoshi Kuroiwa,[6] Olle Terenius,[7] and Hiroyuki Matsuoka[1]

[1]Division of Medical Zoology
Department of Infection and Immunity
Jichi Medical University School of Medicine
Shimotsuke City, Tochigi 329-0498
Japan

[2]Department of Immunology and Parasitology
University of Occupational and Environmental Health, Japan
Kitakyusyu, Fukuoka 807-8555
Japan

[3]Miyagishima Initiative Research Unit
RIKEN Frontier Research System
Wako, Saitama 351-0198
Japan

[4]Department of Tropical Medicine and Parasitology
Dokkyo University School of Medicine
Mibu, Tochigi 321-0293
Japan

[5]Department of Biomedical Chemistry
Graduate School of Medicine
The University of Tokyo
Hongo, Tokyo 113-0033
Japan

[6]Research Information Center for Extremophile
Rikkyo (St. Paul's) University
Toshimaku, Tokyo 171-8501
Japan

[7]Department of Molecular Biology and Biochemistry
University of California
3205 McGaugh Hall
Irvine, California 92697

Summary

Malaria, which is caused by *Plasmodium* parasites, is transmitted by anopheline mosquitoes. When gametocytes, the precursor cells of *Plasmodium* gametes, are transferred to a mosquito, they fertilize and proliferate, which render the mosquito infectious to the next vertebrate host [1]. Although the fertilization of malaria parasites has been considered as a rational target for transmission-blocking vaccines [2], the underlying mechanism is poorly understood. Here, we show that the rodent malaria parasite gene *Plasmodium berghei* GENERATIVE CELL SPECIFIC 1 (PbGCS1) plays a central role in its gametic interaction. *PbGCS1* knockout parasites show male sterility, resulting in unsuccessful fertilization. Because such a male-specific function of GCS1 has been observed in angiosperms [3, 4], this indicates, for the first time, that parasite sexual reproduction is controlled by a machinery common to flowering plants. Our present findings provide a new viewpoint for understanding the parasitic fertilization system and important clues for novel strategies to attack life-threatening parasites.

*Correspondence: mhirai@ms.jichi.ac.jp
[8]These authors contributed equally to this work.

Results and Discussion

GCS1 Is Highly Conserved in *Plasmodium* and Other Organisms

Our previous study revealed that angiosperm GCS1 has an exclusive function in male fertility and that putative *GCS1* genes are widely conserved in various organisms including the human malaria *P. falciparum*, (AAN35337) [3]. To investigate whether malaria GCS1 has a role in parasite fertilization similar to that of angiosperm GCS1, we searched for homologous sequences in the rodent malaria parasite *P. berghei* because this parasite is amenable to gene targeting [5] and its fertilization can be easily evaluated in vitro and in vivo [6]. As a result, the sequence PB000710.01.0 (PlasmoDB) was detected as only one putative *GCS1* candidate (*PbGCS1*). The full-length *PbGCS1* cDNA from the gamete stage was cloned and found to have an N-terminal signal sequence and a C-terminal transmembrane domain, typical of GCS1s (Figure 1A). Further database analysis indicated that *GCS1*s are present in other parasites (*Cryptosporidium parvum*, *Leishmania major*, and *Trypanosoma cruzi*) besides malaria parasites (*P. yoelii* and *P. vivax*) as a single-copy gene. In addition, genomes of amoeba (*Dictyostelium discoideum* and *Physarum polycephalum*) and some animal species (*Monosiga brevicollis*, *Hydra magnipapillata*, and *Nematostella vectensis*) also possess a *GCS1*-like gene. The widespread distribution of *GCS1*-like genes in major eukaryotic kingdoms suggests that the origin of *GCS1*-like genes is close to the origin of eukaryotes [3]. (Figures 1B and 1C).

PbGCS1 Is Expressed in Male Gametocytes and Gametes

To investigate PbGCS1 expression, we generated a transgenic *P. berghei* expressing PbGCS1 fused with Azami Green Fluorescent Protein (AGFP) (PbGCS1::AGFP) under the endogenous *PbGCS1* promoter (Figures 2A and 2B). A subpopulation of erythrocytes infected with *PbGCS1::AGFP* parasites showed fluorescent signals (Figures 2C and 2D). The parasitized blood was incubated in gametogenesis-inducing medium [7] to observe gametocytes and gametes. The exflagellation of PbGCS1::AGFP-expressing cells (>70%) occurred 15 min after induction, indicating that PbGCS1 is expressed in male gametocytes and gametes. Due to the swift motility of male flagella, it was difficult to observe fluorescence in them. To facilitate observation of flagella, the *PbGCS1::AGFP* parasites were immunostained with anti-AGFP antibody. As a result, AGFP signals were detected in both exflagellating male gametes and flagella (Figures 2E–2G). The expression of PbGCS1 also was investigated in female gametes. The *PbGCS1::AGFP* transformants were incubated in gametogenesis-inducing medium under the condition in which their fertilization is inhibited by male inactivation with aphidicolin treatment, whereas females transform into functional gametes [6]. To discriminate the female gametes from AGFP-expressing cells, the transformants

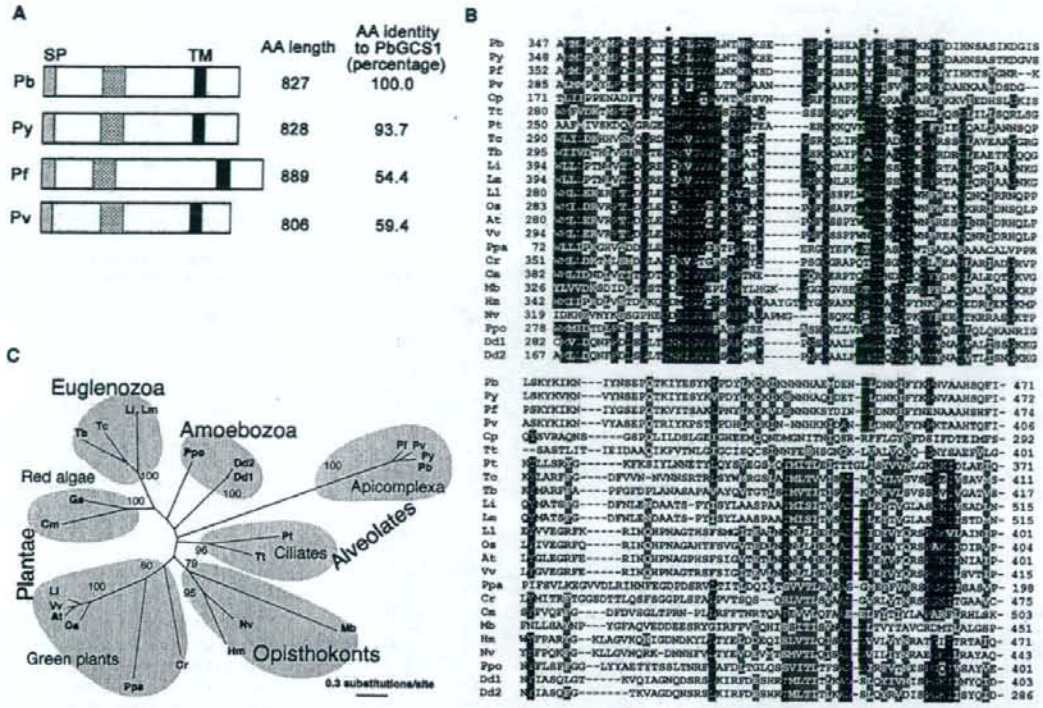

Figure 1. Primary Structure of PbGCS1

(A) GCS1 homologs in *P. berghei* (Pb), *P. yoelii* (Py), *P. falciparum* (Pf), and *P. vivax* (Pv). Abbreviations: SP, putative signal peptide; and TM, transmembrane region. Previously identified conserved regions [3] are indicated by hatched boxes, and alignment is shown in (B).

(B) Comparison of the amino acid sequences conserved among the GCS1 homologs. Identical and conserved residues are shaded black and gray, respectively. Notably, three cysteine residues are completely conserved among all homologs (asterisks).

(C) A maximum-likelihood tree of GCS1 homologs. The tree includes sequences of kinetoplastids (Euglenozoa; Tb, Tc), Amoebozoa (Ppo, Dd), ciliates (Alveolata; Pt, Tt), Apicomplexa (Alveolata; Pt, Pv, Py, Pb), animals (Opisthokonta; Hm, Nv) Choanozoa (Opisthokonta; Mb), plants (green plants in Plantae; Ll, Vv, At, Os, Ppa), a green alga (green plants in Plantae; Cr), and red algae (Plantae; Cm, Gs). A deduced GsGCS1 sequence was obtained from the *Galdieria sulphuraria* genome project (http://genomics.msu.edu/cgi-bin/galdieria/blast.cgi). Numbers at the nodes are local bootstrap values calculated by using PhyML analyses. Bootstrap values >75% are shown at the selected nodes. Branch lengths are proportional to the number of amino acid substitutions, which are indicated by the scale bar below the tree. Abbreviations: At, *Arabidopsis thaliana*; Cm, *Cyanidioschyzon merolae*; Cp, *Cryptosporidium parvum*; Cr, *Chlamydomonas reinhardtii*; Dd, *Dictyostelium discoideum*; Gs, *Galdieria sulphuraria*; Hm, *Hydra magnipapillata*; Li, *Leishmania infantum*; Ll, *Lilium longiflorum*; Lm, *Leishmania major*; Mb, *Monosiga brevicollis*; Nv, *Nematostella vectensis*; Os, *Oryza stiva*; Ppa, *Physcomitrella patens*; Ppo, *Physarum polycephalum*; Tb, *Trypanosoma brucei*; Tc, *Trypanosoma cruzi*; Tt, *Tetrahymena thermophila*; Pt, *Paramecium tetraurelia*; and Vv, *Vitis vinifera*.

were immunostained with AGFP antibody and a monoclonal antibody against Pbs21, which is a marker protein for female gametes, zygotes, and ookinetes [8]. By observing more than 150 female gametes obtained from at least three independent experiments, we confirmed that all Pbs21-positive female gametes were AGFP-negative and vice versa. This suggests that PbGCS1 is not expressed in female gametes (Figures 2H–2K). These observations indicate that the *GCS1* gene is likely to be exclusively expressed in the male gametocytes and gametes. Next, we investigated the PbGCS1 expression in ookinetes, which is a postfertilization stage. To avoid any adverse effects caused by the PbGCS1 modifications, a transgenic *P. berghei* expressing AGFP under the *PbGCS1* promoter was generated (*PbGCS1prom::AGFP*) (Figures S1A and S1B available online). The transformants underwent normal asexual and sexual stage development in vivo and showed male specific AGFP expression (Figure S1C), whereas no fluorescent signal was detected in ookinetes (Figure S1D). Taken together, *PbGCS1* is expressed only in male gametocytes and gametes, and its expression level is rapidly decreased after fertilization.

PbGCS1 Is Essential for Parasite Fertilization

To address the PbGCS1 functions, we generated *PbGCS1*(−) *P. berghei* (Figure 3A) and performed phenotypic analyses. Three independent clones (1–3, 2–5, and 3–6) were established, and the correct targeting event in each clone was confirmed by diagnostic PCR and Southern blot analysis (Figures 3B and 3C). The morphology of *PbGCS1*(−) gametocytes was indistinguishable from normal parasites (Figure 3D). *PbGCS1*(−) parasites underwent normal development of asexual blood stages and gametocyte formation in mice (further described in Table S1).

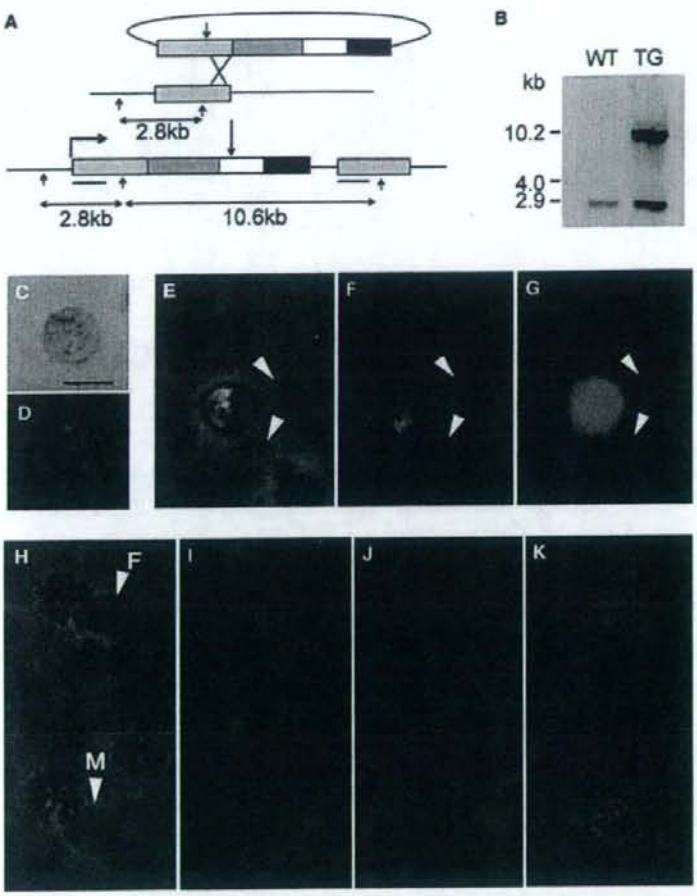

Figure 2. Generation and Characterization of the Transgenic Parasite Line *PbGCS1::AGFP*

(A) Schematic representation of AGFP tagging of the *PbGCS1* locus using a plasmid that integrated through single crossover homologous recombination. The boxes indicate *PbGCS1* gene (gray), *AGFP* (green), 3′ UTR of *PbGCS1* gene (white) and *TgDHFR/ts* selectable marker (black). "E" indicates EcoRI digestion site. For the transfection experiment, the plasmid was cut with the EcoRI site in the *PbGCS1* gene. Bars represent the position of the probe used in Southern blot analysis.

(B) Southern blot genotyping confirmed gene integration. Hybridization of the probe with EcoRI-digested genomic DNA yielded a 2.8 kb WT and 2.8 and 10.6 kb transgenic (TG) bands.

(C) Live PbGCS1::AGFP-expressing cells.

(D) The fluorescent signal of the same cell in (C).

(E–G) An exflagellating male was immunostained with anti-AGFP antibody. (E) Bright field. (F) Nuclear staining with DAPI. (G) PbGCS1::AGFP expression. Arrows indicate flagella being released.

(H–K) The gametes from the transgenic line were double stained with anti-Pbs21 (I) and anti-AGFP (J). "F" and "M" in (H) indicate female and male gamete, respectively. Bars represent 5 μm.

We investigated the infectivity of *PbGCS1*(−) parasites for mosquitoes and subsequent transmission to mice. As control knockout parasites possess wild-type *PbGCS1*, we generated *Pbs21*(−) parasites [9] and used them for this study. It is known that *Pbs21*(−) parasites develop normally in the blood stages and show normal infectivity for mosquitoes and transmission to mice [9, 10]. *Anopheles stephensi* mosquitoes were fed on infected mice carrying either *PbGCS1*(−) or *Pbs21*(−) parasites, which were then dissected for the evaluation of parasite development at day 16 postfeeding. Three independent experiments showed that oocysts (in the midgut) and sporozoites (in the salivary glands) were detected in the mosquitoes fed on mice carrying *Pbs21*(−) parasites. In sharp contrast, no oocyst nor sporozoite was detected in the mosquitoes fed on mice carrying *PbGCS1*(−) parasites (Figures 3E and 3F and Table S2). When naive mice were subjected to these mosquitoes' bites, only *Pbs21*(−) parasites appeared in the mouse blood, indicating that development of *PbGCS1*(−) parasites was completely halted at the mosquito stage (Figure 3E and Table S2). These results indicate that PbGCS1 is essential for the mosquito stages of development.

In *P. berghei*, an in vitro assay has been established that mimics the gametogenesis and fertilization taking place in the mosquito body [6]. By using this system, it was found that the efficiency of male gametogenesis in *PbGCS1*(−) parasites was comparable to that of *Pbs21*(−) parasites (Figure 4A and Table S1). In *Pbs21*(−) parasites, female gametes fertilized with male gametes and then transformed into ookinetes (Figure 4A). In *PbGCS1*(−) parasites, on the other hand, female gametes did not fertilize with males, resulting in 86% of female gametes, which were forming clumps, remaining unfertilized (Figures 4A and 4C). These results clearly indicate that PbGCS1 is involved in the interaction process between male and female gametes.

PbGCS1 Determines Male Fertility of Parasites

As shown in the analysis based on AGFP marker lines, PbGCS1 is expressed in the male gametocytes and gametes. Therefore, the fertilization failure observed in *PbGCS1*(−) parasites likely was attributed to male sterility. To confirm this possibility, we performed two sets of in vitro crossfertilizations between *PbGCS1*(−) and *Pbs21*(−) gametes and two sets of self-fertilizations of *Pbs21*(−) and *PbGCS1*(−) gametes as control experiments. Control experiments showed that self-fertilization of *PbGCS1*(−) parasites did not produce any ookinetes, whereas that of *Pbs21*(−) parasites did (Figure 4B). Because the *Pbs21*gene is inactive in *Pbs21*(−) parasites, ookinetes generated from *Pbs21*(−) self-fertilization did not express Pbs21 protein, which was confirmed by immunostaining (Figure 4B and left panels in Figure 4D). As in the first crossfertilization experiment, *PbGCS1*(−) female gametes were crossed with *Pbs21*(−) male/female gametes. As a result,

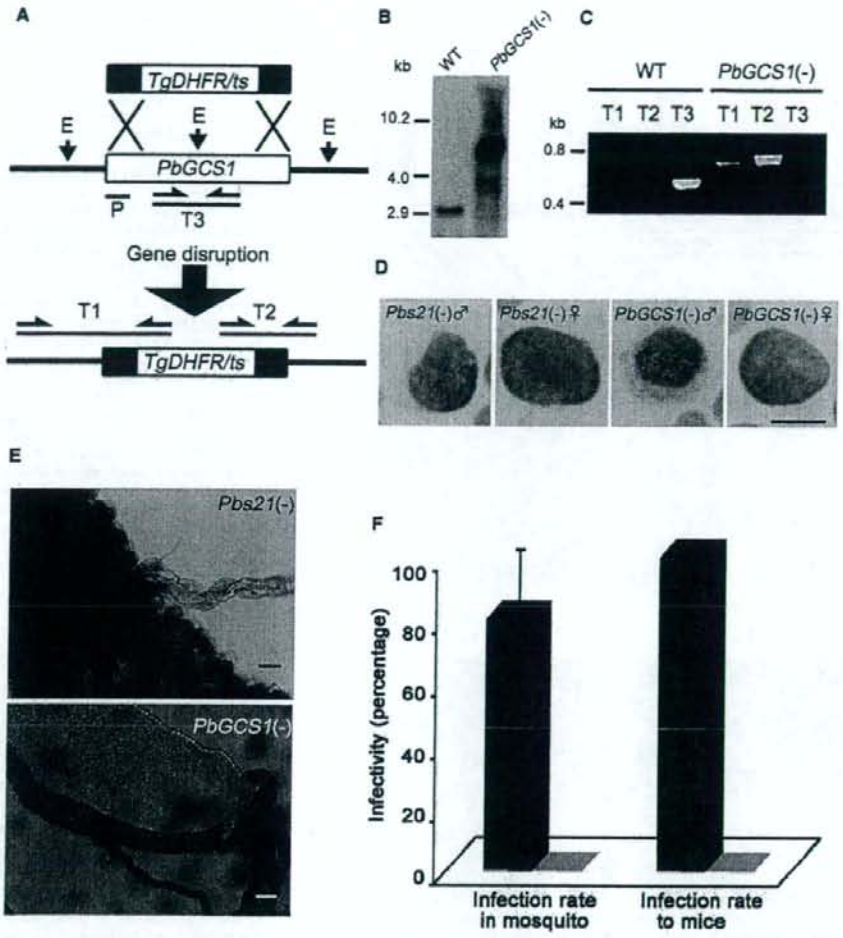

Figure 3. Targeted Disruption of the *PbGCS1* Gene and Resulting Phenotypes of *PbGCS1*(−) *P. berghei*

(A) Schematic representation of replacement strategy to generate *PbGCS1*(−) parasites. The WT *PbGCS1* genomic locus is replaced with 5′ and 3′ regions of *PbGCS1*(−) open reading frame and *TgDHFR*, a selectable marker. "E" and "P" indicate EcoRI sites and the probe region used for the Southern blot analysis shown in (B), respectively. The bars labeled with T1-3 indicate amplified regions by the diagnostic PCRs in (C).

(B) Southern blot analysis of WT and *PbGCS1*(−) parasites.

(C) Diagnostic PCRs. The bands in T1/T2 and T3 are specific to *PbGCS1*(−) and WT parasites, respectively.

(D) *PbGCS1*(−) and *Pbs21*(−) gametocytes were stained with Giemsa. Bar represents 5 μm.

(E) Mosquito midguts infected with *Pbs21*(−) and *PbGCS1*(−) parasites. The latter carries no oocyst. Bars represent 50 μm.

(F) The infection rate and transmission efficiency of *Pbs21*(−) (dark gray bar) and *PbGCS1*(−) (light gray bar). Error bars represent mean ± SD (n = 3). The details are shown in Table S2.

Pbs21-positive (55%) and -negative (45%) ookinetes were produced (Figure 4B and right panels in Figure 4D). In this experiment, Pbs21-negative ookinetes were derived from self-fertilization of *Pbs21*(−) gametes, whereas Pbs21-positive ookinetes were only produced by crossfertilization between *PbGCS1*(−) (namely *Pbs21*[+]) females and *Pbs21*(−) (namely *PbGCS1*[+]) males. This result indicates that *PbGCS1*(−) female gametes are fertile and that disruption of the *PbGCS1* gene does not affect the parasite development after fertilization. As the second crossfertilization experiment, *PbGCS1*(−) male/female gametes were crossed with *Pbs21*(−) females, resulting in no ookinetes (Figure 4B and Table S3). This indicates that *PbGCS1*(−) males failed to fertilize with Pbs21(−) females. The fertilization failure of *PbGCS1*(−) males was not complemented by *Pbs21*(−) (namely *PbGCS1*[+]) females (the results of the in vitro fertilization assay are summarized in Figure S2). We tested the possibility that PbGCS1 may have a role in flagellum motility. The *PbGCS1*(−)

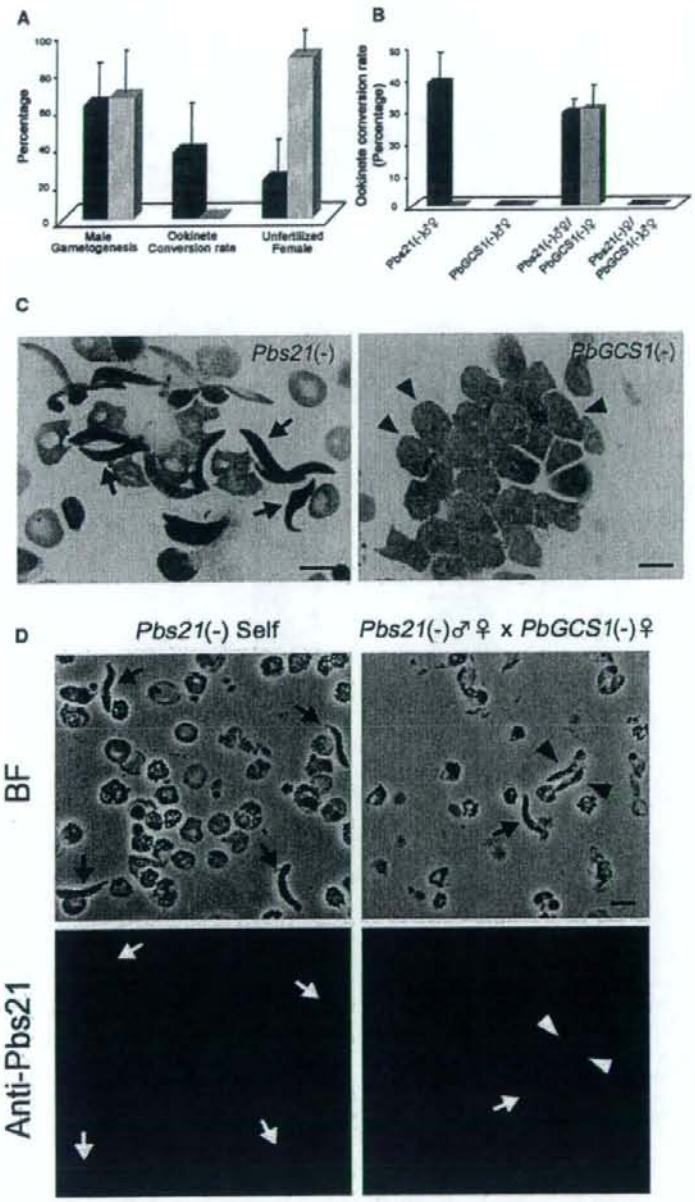

Figure 4. Fertility of *PbGCS1*(−) Parasites

(A) The rates of ♂ gametogenesis, ookinete formation, and unfertilized ♀ gametes of *PbGCS1*(−) (light gray bar) and *Pbs21*(−) (dark gray bar) are indicated. Error bars represent mean ± SD (n = 3). The details are shown in Table S1.

(B) The Pbs21-negative (dark gray bar) and -positive (light gray bar) ookinetes resulting from each mating combination were counted. *Pbs21*(−)♂♀ and *PbGCS1*(−)♂♀ indicate self-fertilization of each line. Error bars represent mean ± SD (n = 3). The details are shown in Table S3.

(C) Transgenic parasites cultured for 16 hr after gametogenesis induction were stained with Giemsa. Many ookinetes were observed in *Pbs21*(−) (exemplified by arrow in left panel), whereas clumps of unfertilized ♀ gametes with no ookinete are seen in *PbGCS1*(−) (arrowhead in right panel). Bars represent 5 μm.

(D) Ookinetes produced by *Pbs21*(−) self-fertilization (left panels) and those by crossfertilization of *PbGCS1*(−) ♀ and *Pbs21*(−) ♂/♀ gametes (right panels) were immunostained with anti-Pbs21 antibody. *Pbs21*(−) ookinetes (indicated with arrows in the left panels) do not show fluorescent signal for Pbs21. Both Pbs21-positive (arrowheads in the right panels) and -negative (arrow in the right panels) ookinetes are produced by crossfertilization. Bars represent 5 μm.

male gametes showed flagella motility and adhesion to surrounding erythrocytes, forming exfagellating centers, all of which were comparable to that of *Pbs21*(−) gametes. However, no successful entering of flagella into female gametes was observed in *PbGCS1*(−) (Movies S1 and S2). Taken together, we conclude that PbGCS1 has a male-specific function during the interaction with female gametes, and, therefore, that PbGCS1 is indispensable for parasite fertilization.

GCS1-Based Fertilization May Be Highly Conserved in Various Organisms

In the present report, we show that PbGCS1, which was initially identified as a putative ortholog to angiosperm GCS1, is surely functional in malaria parasite reproduction. This demonstrates that mechanisms for parasite fertility are, at least in part, common to that of plant fertilization. It is widely accepted that the phylum Apicomplexa, including malaria parasites, is evolved from secondary endosymbiosis of red algae, from which malaria parasites acquired plastids, nonphotosynthetic chloroplasts called "apicoplasts" [11]. Some basic metabolic pathways of malaria parasites (for example, fatty acid synthesis and ferredoxin-dependent redox systems) are encoded by the apicoplast genome. These processes, therefore, show plant-type characteristics derived from red algal plastid metabolisms [12]. The parasite reproduction based on GCS1 probably is not derived from the engulfed red alga because we could not detect any remarkable close relationships of *GCS1* genes between Apicomplexa and red algae in the phylogenetic analysis (Figure 1C). However, it is still possible that the fast-evolving apicomplexan genes mislead their position in the phylogenetic tree. Nevertheless, putative GCS1 orthologs also exist in amoebozoan and opisthokont species, which have not experienced the primary endosymbiosis of cyanobacteria nor secondary endosymbiosis of eukaryotic algae [13] (Figures

1B and 1C), suggesting that the ancestor of malaria parasites already had the *GCS1* gene before the acquisition of the apicoplast by the red algal secondary endosymbiosis. Given that both plant and apicomplexan *GCS1* genes are involved in fertilization, it is most likely that the original function of GCS1 was in the fertilization of the ancestral eukaryotes.

Besides the conservation of GCS1 possession, our previous study has shown that *C. reinhardtii* and *P. polycephalum* display gamete-specific GCS1 expression at the transcription level, and the expression is dramatically reduced after mating in both organisms [3]. The similar expression pattern also was confirmed in PbGCS1, where the PbGCS1::AGFP protein is expressed in male gametocytes and gametes and the expression is reduced in ookinetes, a postfertilization stage. Such a similarity in stage-specific expression of GCS1 in malaria parasites, plants, algae, and slime mold strongly suggests that GCS1 may function in a similar fashion in these organisms. If this is the case, comparative studies of GCS1 in each organism will accelerate our understanding of the mechanisms involved in fertilization. In addition, there is urgent need for effective strategies to attack parasites threatening humans. The mosquito-parasite interaction has been recognized as a target of transmission-blocking strategies. Several candidate molecules involved in this interaction have been found in gametes, zygotes, and ookinetes and have been tested for their ability to block transmission [2]. For this purpose, the gametic interaction is a novel target. It is worth exploring the possibility of whether GCS1-attacking approaches could be a new antiparasite strategy without affecting the host's reproduction because an obvious GCS1 homolog has not been detected in mammalians.

Experimental Procedures

Plasmid Construction

Procedures for construction of *PbGCS1::AGFP* and *PbGCS1prom::AGFP* plasmids, and primer sequences used in this study are described in the Supplemental Data.

Generation of *PbGCS1* Knockout Parasites

For disruption of *PbGCS1*, two *P. berghei* (ANKA clone 2.34) genomic fragments covering the *PbGCS1* coding region were amplified with two sets of primers (GCS1-F1-HindIII/GCS1-R1-HindIII and GCS1-F2-EcoRI/GCS1-R2-BamHI). Cloning these fragments into the *P. berghei* targeting vector pBS-DHFR [14] resulted in the plasmid pPbGCS1-KO. The transfection, pyrimethamine selection, and dilution cloning were performed as described [15]. Three *PbGCS1*(−) clones (1–3, 2–5, and 3–6) from three independent transfection experiments were obtained. The expected recombination event in each clone was confirmed by diagnostic PCR. For Southern blot analyses, a DNA fragment amplified with primers (PbGCS1-F1/PbGCS1-R1) and *P. berghei* genomic DNA was labeled with AlkPhos Direct Labeling Kit (GE Healthcare Bioscience) and used as a probe.

Assessment of Blood Stage Development and Fertility

Thin blood films prepared from mice infected with either *PbGCS1*(−) or *Pbs21*(−) parasites were stained with Giemsa, on which parasitemia, gametocytemia, and sex ratio were calculated. To evaluate the efficiency of fertilization and subsequent development into ookinetes, infected blood was mixed with gametogenesis-inducing medium to induce gamete formation; then, the number of exflagellating males was counted at 15 min after induction. The sample was further cultured for 16 hr, when the number of ookinetes was counted. Sex-specific involvement of PbGCS1 in sexual reproduction was analyzed by a crossfertilization assay as described below.

Infectivity of Parasite for Mosquitos and Transmission to Mice

Anopheles stephensi were reared as previously described [16] and infected with parasites as described [5]. In brief, female mosquitoes (4–7 days old) were fed on mice carrying either *Pbs21*(−) or *PbGCS1*(−) parasites, and fully engorged mosquitoes were collected. Sixteen days after blood feeding, ten mosquitoes were dissected, and midguts and salivary glands were isolated. The number of oocysts on the midgut and the presence of sporozoites in the salivary glands was examined. The rest of the mosquitoes were fed on naive Balb/c mice. The transmission of parasites from mosquitoes to mice was examined by checking mouse blood smears every day for 2 weeks after the feeding.

In Vitro Crossfertilization Assay

The in vitro crossfertilization assay was performed as previously described [6]. Five μl of tail blood from a mouse infected with parasite clone A (*PbGCS1*[−] or *Pbs21*[−] parasites) was immediately added to 1 ml of gametogenesis-inducing medium (10% fetal bovine serum in RPMI1640, pH 8.2) containing 500 μM of aphidicolin at 21°C for 12 min to induce female gamete formation. Aphidicolin inhibits male gamete formation, whereas female gametes are formed normally. At the same time, 5 μl of tail blood from a mouse infected with clone B (*PbGCS1*[−] or *Pbs21*[−] parasites) was added immediately into 1 ml of gametogenesis-inducing medium at 21°C for 12 min without aphidicolin. Clone A was centrifuged, and the supernatant removed. The suspension of clone B was added to the pellet of clone A and mixed. This mixture was further incubated for 16 hr to induce fertilization and ookinete formation. The ookinete conversion rate was determined by the percentage of female gametocytes of clone A that fertilized with male gametes of clone B and transformed into ookinetes. Ookinetes were immunostained with anti-Pbs21 monoclonal antibody as described in the Supplemental Data.

Accession Numbers and Phylogenetic Study

See the Accession Numbers section for information on the *PbGCS1* cDNA sequence. The accession numbers of other GCS1s are *C. parvum* (XP_627125), *T. thermophila* (XP_001030543), *P. tetraurelia* (XP_001431224), *T. cruzi* (XP_814894), *T. brucei* (XP_823296), *L. infantum* (XP_001468864), *L. major* (XP_843157), *C. merolae* (AP006493), *P. polycephalum* (BAE71144), *L. longiflorum* (BAE71142), A. thaliana (BAE71143), *O. stiva* (NP_001055054), *C. reinhardtii* (XP_001695893). *V. vinifera* (CAO63696), *P. patens* (XP_001770778), *M. brevicollis* (XP_001746497), *H. magnipapillata* (ABN45755), *N. vectensis* (XP_001628495), and *D. discoideum* (Dd1, XP_643321; Dd2, AAS45348). Phylogenetic analysis using these sequences is described in the Supplemental Data.

Accession Numbers

The GenBank accession number for the *PbGCS1* cDNA sequence reported in this paper is EU369602.

Supplemental Data

Supplemental Experimental Procedures, two figures, three tables, and two movies are available at http://www.current-biology.com/cgi/content/full/18/8/607/DC1/.

Acknowledgments

This research was supported by a Grant-in-Aid for Young Scientists (B) (M.H.), for Exploratory Research (M.A.), and for Scientific Research (B) (H.M.) from the Japan Society for the Promotion of Science, the Special Postdoctoral Researchers Program of Riken (T.M.), the Program for the Promotion of Basic Research Activities for Innovative Biosciences (T.K.), and Creative Scientific Research from the Japanese Ministry of Education, Science, Culture, Sports, and Technology (K.K.).

Received: February 8, 2008
Revised: March 10, 2008
Accepted: March 20, 2008
Published online: April 10, 2008

References

1. Baton, L.A., and Ranford-Cartwright, L.C. (2005). Spreading the seeds of million-murdering death: metamorphoses of malaria in the mosquito. Trends Parasitol. *21*, 573–580.
2. Sauerwein, R.W. (2007). Malaria transmission-blocking vaccines: the bonus of effective malaria control. Microbes Infect. *9*, 792–795.

3. Mori, T., Kuroiwa, H., Higashiyama, T., and Kuroiwa, T. (2006). GENERATIVE CELL SPECIFIC 1 is essential for angiosperm fertilization. Nat. Cell Biol. *8*, 64–71.
4. von Besser, K., Frank, A.C., Johnson, M.A., and Preuss, D. (2006). Arabidopsis HAP2 (GCS1) is a sperm-specific gene required for pollen tube guidance and fertilization. Development *133*, 4761–4769.
5. Hirai, M., Arai, M., Kawai, S., and Matsuoka, H. (2006). PbGCβ is essential for Plasmodium ookinete motility to invade midgut cell and for successful completion of parasite life cycle in mosquitoes. J. Biochem. (Tokyo) *140*, 747–757.
6. van Dijk, M.R., Janse, C.J., Thompson, J., Waters, A.P., Braks, J.A., Dodemont, H.J., Stunnenberg, H.G., van Gemert, G.J., Sauerwein, R.W., and Eling, W. (2001). A central role for P48/45 in malaria parasite male gamete fertility. Cell *104*, 153–164.
7. Winger, L.A., Tirawanchai, N., Nicholas, J., Carter, H.E., Smith, J.E., and Sinden, R.E. (1988). Ookinete antigens of Plasmodium berghei. Appearance on the zygote surface of an Mr 21 kD determinant identified by transmission-blocking monoclonal antibodies. Parasite Immunol. *10*, 193–207.
8. Paton, M.G., Barker, G.C., Matsuoka, H., Ramesar, J., Janse, C.J., Waters, A.P., and Sinden, R.E. (1993). Structure and expression of a post-transcriptionally regulated malaria gene encoding a surface protein from the sexual stages of Plasmodium berghei. Mol. Biochem. Parasitol. *59*, 263–275.
9. Tomas, A.M., Margos, G., Dimopoulos, G., van Lin, L.H.M., de Koning-Ward, T.F., Sinha, R., Lupetti, P., Beetsma, A.L., Rodriguez, M.C., Karras, M., et al. (2001). P25 and P28 proteins of the malaria ookinete surface have multiple and partially redundant functions. EMBO J. *20*, 3975–3983.
10. Sidén-Kiamos, I., Vlachou, D., Margos, G., Beetsma, A., Waters, A.P., Sinden, R.E., and Louis, C. (2000). Distinct roles for pbs21 and pbs25 in the in vitro ookinete to oocyst transformation of Plasmodium berghei. J. Cell Sci. *113*, 3419–3426.
11. Foth, B.J., and McFadden, G.I. (2003). The apicoplast: a plastid in Plasmodium falciparum and other Apicomplexan parasites. Int. Rev. Cytol. *224*, 57–110.
12. Kimata-Ariga, Y., Kurisu, G., Kusunoki, M., Aoki, S., Sato, D., Kobayashi, T., Kita, K., Horii, T., and Hase, T. (2007). Cloning and characterization of ferredoxin and ferredoxin-NADP+ reductase from human malaria parasite. J. Biochem. (Tokyo) *141*, 421–428.
13. Reyes-Prieto, A., Weber, A.P., and Bhattacharya, D. (2007). The origin and establishment of the plastid in algae and plants. Annu. Rev. Genet. *41*, 147–168.
14. Dessens, J.T., Beetsma, A.L., Dimopoulos, G., Wengelnik, K., Crisanti, A., Kafatos, F.C., and Sinden, R.E. (1999). CTRP is essential for mosquito infection by malaria ookinetes. EMBO J. *18*, 6221–6227.
15. Janse, C.J., Ramesar, J., and Waters, A.P. (2006). High-efficiency transfection and drug selection of genetically transformed blood stages of the rodent malaria parasite Plasmodium berghei. Nat. Protocols *1*, 346–356.
16. Hirai, M., Wang, J., Yoshida, S., Ishii, A., and Matsuoka, H. (2001). Characterization and identification of exflagellation-inducing factor in the salivary gland of Anopheles stephensi (Diptera: Culicidae). Biochem. Biophys. Res. Commun. *287*, 859–864.

Coinfection with Nonlethal Murine Malaria Parasites Suppresses Pathogenesis Caused by *Plasmodium berghei* NK65

Mamoru Niikura,[1]*‡ Shigeru Kamiya,† Kiyoshi Kita,‡ and Fumie Kobayashi[1]†

Mixed infection with different *Plasmodium* species is often observed in endemic areas, and the infection with benign malaria parasites such as *Plasmodium vivax* or *P. malariae* has been considered to reduce the risk of developing severe pathogenesis caused by *P. falciparum*. However, it is still unknown how disease severity is reduced in hosts during coinfection. In the present study, we investigated the influence of coinfection with nonlethal parasites, *P. berghei* XAT (*Pb* XAT) or *P. yoelii* 17X (*Py* 17X), on the outcome of *P. berghei* NK65 (*Pb* NK65) lethal infection, which caused high levels of parasitemia and severe pathogenesis in mice. We found that the simultaneous infection with nonlethal *Pb* XAT or *Py* 17X suppressed high levels of parasitemia, liver injury, and body weight loss caused by *Pb* NK65 infection, induced high levels of reticulocytemia, and subsequently prolonged survival of mice. In coinfected mice, the immune response, including the expansion of $B220^{int}CD11c^{+}$ cells and $CD4^{+}$ T cells and expression of IL-10 mRNA, was comparable to that in nonlethal infection. Moreover, the suppression of liver injury and body weight loss by coinfection was reduced in IL-$10^{-/-}$ mice, suggesting that IL-10 plays a role for a reduction of severity by coinfection with nonlethal malaria parasites. *The Journal of Immunology*, 2008, 180: 6877–6884.

Malaria is the infectious disease that causes incidence estimates of 2–3 million deaths and 300–500 million clinical cases in the world (1). There are four species of *Plasmodium* that infect humans: *Plasmodium falciparum*, *Plasmodium vivax*, *Plasmodium malariae*, and *Plasmodium ovale*. *P. falciparum* is the major human parasite responsible for high morbidity and mortality, and infection with *P. falciparum* is associated with developing fever, a high number of parasites in the blood, and pathogenesis, including severe anemia, body weight loss, and cerebral malaria in humans (2). The sensitive PCR-based techniques have revealed that coinfection with different *Plasmodium* species is common in developing countries (3, 4). In particular, the simultaneous presence of *P. vivax* or *P. malariae* during *P. falciparum* infection is often observed when the prevalence of *Plasmodium* infections in humans is analyzed in endemic areas (5–7) and it is known to reduce the risk of developing a high number of parasites in the blood as well as pathogenesis (8–11).

Murine malaria models have been used for understanding the induction of immune interaction in hosts and investigating factors associated with malarial defense mechanism. Coinfection with two different species and/or strains of murine malaria parasites has been shown to influence the parasitemia or mortality of each other (12). The development of experimental cerebral malaria caused by *Plasmodium berghei* (*Pb*)[2] ANKA was inhibited by the simultaneous presence of *Plasmodium yoelii yoelii* or *P. berghei* K173 (13, 14). However, it is still unknown how the disease severity is suppressed in simultaneous infection.

In the present study, we investigated the influence of simultaneous infection with nonlethal parasites, *P. berghei* XAT (*Pb* XAT) or *P. yoelii* 17X (*Py* 17X), on the outcome of *P. berghei* NK65 (*Pb* NK65) lethal infection, which causes high levels of parasitemia and pathogenesis such as body weight loss and liver injury in mice. First, we found that *Pb* XAT-immunized mice acquired resistance to *Pb* NK65 infection, although *Py* 17X-immunized mice were susceptible to *Pb* NK65 infection. By using these three species and strains, we examined how *Pb* XAT or *Py* 17X nonlethal infection modulated the immune responses such as cytokine production and cellular expansion during *Pb* NK65 lethal infection.

Materials and Methods

Mice

Female C57BL/6 (B6) mice were purchased from CLEA Japan and used at 5–6 wk of age. IL-$10^{-/-}$ mice on B6 background were purchased from The Jackson Laboratory. We used 20- to 24-wk-old female IL-$10^{-/-}$ mice (experiment 1), 5- to 6-wk-old male or female IL-$10^{-/-}$ mice (experiment 2), and age-matched female B6 mice in these studies. The genotype of female IL-$10^{-/-}$ mice used in experiments was verified by PCR. The experiments were approved by the Experimental Animal Ethics Committee at Kyorin University, and all experimental animals were kept on the specific pathogen-free unit at the animal facility with sterile bedding, food, and water.

Parasites and infections

Malaria parasites were stored as frozen stocks in liquid nitrogen. *Pb* NK65 is a high-virulence strain and was originally obtained from Dr. M. Yoeli (New York University Medical Center, New York, NY). *Pb* XAT is a low-virulence derivative from *Pb* NK65 (15). A nonlethal isolate of *Py* 17X was originally obtained from Dr. J. Finnerty (National Institutes of Health, Bethesda, MD) and cloned by limiting dilution. Parasitized RBCs (pRBCs) of *Pb* NK65, *Pb* XAT, and *Py* 17X were generated in donor mice inoculated i.p. with each frozen stock of parasites. The donor mice were monitored for parasitemia daily and bled for experimental infection in ascending periods of parasitemia. Experimental mice were infected i.v. with 1×10^4 pRBCs of a given parasite species or strain. Therefore, when mice were coinfected with two species/strains of parasites, a total of 2×10^4 pRBCs (1×10^4 of each parasite species/strain) were inoculated.

*Institute of Laboratory Animals, Graduate School of Medicine and †Department of Infectious Diseases, Faculty of Medicine, Kyorin University, Tokyo; and ‡Department of Biomedical Chemistry, Graduate School of Medicine, University of Tokyo, Tokyo, Japan

Received for publication July 12, 2007. Accepted for publication March 4, 2008.

The costs of publication of this article were defrayed in part by the payment of page charges. This article must therefore be hereby marked *advertisement* in accordance with 18 U.S.C. Section 1734 solely to indicate this fact.

[1] Address correspondence and reprint requests to Dr. Fumie Kobayashi and Dr. Mamoru Niikura, Faculty of Medicine, Kyorin University, 6-20-2 Shinkawa, Mitaka, Tokyo 181-8611, Japan. E-mail addresses: fumfum@ks.kyorin-u.ac.jp and mniikura@ks.kyorin-u.ac.jp

[2] Abbreviations used in this paper: *Pb*, *Plasmodium berghei*; *Py*, *Plasmodium yoelii*; pRBC, parasitized RBC; AST, aspartic aminotransferase; ALT, alanine aminotransferase.

Table I. *Total spleen cell number in uninfected and infected mice ($\times 10^8$)*[a]

	Days Postinfection			
	0	6	9	15
Uninfected	0.35 ± 0.17			
Pb NK65		1.05 ± 0.16	0.62 ± 0.25	
Pb XAT		0.74 ± 0.08	2.94 ± 0.75	4.41 ± 1.61
Pb NK65/*Pb* XAT		0.74 ± 0.10	2.22 ± 0.70	6.52 ± 0.98
Py 17X		0.99 ± 0.18	4.63 ± 0.77	10.4 ± 3.02
Pb NK65/*Py* 17X		1.28 ± 0.02	4.63 ± 1.34	11.6 ± 3.48

[a] Mice were infected with malarial parasites as described in the legend to Fig. 2. Spleens were obtained from uninfected and infected mice on days 6, 9, and 15 after infection. Results are expressed as means ± SD of three mice. Experiments were performed three times with similar results.

Parasitemia

Parasitized RBCs were observed by microscopic examination of methanol-fixed tail blood smears stained for 45 min with 1% Giemsa diluted in phosphate buffer (pH 7.2). The number of pRBCs in 250 RBCs was enumerated when parasitemia exceeded 10%, whereas 1×10^4 RBCs were examined when mice showed lower parasitemia. The percentage of parasitemia was calculated as follows: [(No. of pRBCs)/(Total no. of RBCs counted)] × 100.

Measurement of body weights, hematocrits, and circulating reticulocytes

Body weights were measured by balance for animals (KN-661; Natume), and body weight loss was expressed as a percentage of the day 0 value. For hematocrit measurement, tail blood (50 μl) was collected into a heparinized capillary tube and centrifuged at 13,000 × rpm for 5 min with a micro hematocrit centrifuge (HC-12A; Tomy). The hematocrit value was expressed as a percentage of the total blood volume. Reticulocytes in 250 RBCs were counted when reticulocytemia exceeded 20%, whereas 1×10^4 RBCs were examined when mice showed lower reticulocytemia. The percentage of reticulocytemia was calculated as follows: [(No. of reticulocytes)/(Total no. of RBCs counted)] × 100.

Histological examination and measurement of parameters of liver injury

Livers were obtained from infected mice on day 9 postinfection and fixed in 10% buffered formalin and embedded in paraffin. Six-micrometer-thick sections were stained with H&E. The blood was obtained from infected mice on day 9 and centrifuged at 500 × *g* for 10 min. The resulting supernatants were stored at −20°C and used as plasma. The levels of aspartic aminotransferase (AST) and alanine aminotransferase (ALT) in plasma were determined at Nagahama Life Science Laboratory (Shiga, Japan).

Flow cytometry

Flow cytometric analysis was performed on single-cell suspensions of spleen and peripheral blood cells as described previously (16). Total spleen cell numbers in uninfected and infected mice are shown in Table I. The following mAbs were used for analysis: FITC-conjugated anti-CD3ε mAb (clone 145-2C11; eBioscience) and anti-CD4 mAb (clone RM4–5; eBioscience); PE-conjugated anti-CD11c mAb (clone N418; Miltenyi Biotec); allophycocyanin-conjugated anti-CD3ε mAb (clone 145–2C11; eBioscience); and biotin-conjugated anti-CD45R mAb (B220; clone RA3–6B2; BD Pharmingen). MAbs were added to cells in FACS buffer (1% BSA, 0.1% sodium azide in PBS) and incubated at 4°C for 30 min and the cells were washed with cold FACS buffer by centrifugation at 250 × *g* for 2 min. Biotinylated mAbs were followed by streptavidin-conjugated allophycocyanin (4°C, 30 min). After washing with FACS buffer, cells were fixed with 1% paraformaldehyde. Two-color flow cytometry was performed and analyzed with a FACSCalibur (BD Biosciences) using a FlowJo software (version 7.1.3, for Windows).

Detection of cytokine mRNA in spleens

Spleens were removed from infected mice on day 9 postinfection and total RNA was isolated by Isogen (Nippon Gene) according to the manufacturer's protocol. The splenic RNA was reverse-transcribed by murine leukemia virus reverse transcriptase (Applied Biosystems) using random hexamer primers, and reverse transcriptase reaction was preformed at 70°C for 10 min, at 25°C for 10 min, and at 42°C for 30 min. The reaction was terminated by heating at 99°C for 5 min, and the cDNA products were stored at −20°C until use. The 50 μl PCR mixture contained 1 × TaKaRa Ex *Taq* buffer, 2.5 mM dNTP, 1 μl cDNA products, 5 U/μl TaKaRa Ex *Taq* DNA polymerase, and 0.25 μM of PCR primers. The primers used for PCR amplification were as follows: IL-10, 5′-GTG AAG ACT TTC TTT CAA ACA AAG, 3′-CTG CTC CAC TGC CTT GCT CTT ATT; IFN-γ, 5′-TAC TGC CAC GGC ACA GTC ATT GAA, 3′-GCA GCG ACT CCT TTT CCG CTT CCT T; β-actin, 5′-CCA GCC TTC CTT CCT GGG TA, 3′-CTA GAA GCA TTT GCG GTG CA. Thirty cycles of PCR were performed on a thermal cycler (iCycler; Bio-Rad). Each cycle consisted of 30 s of denaturation at 94°C, 30 s of annealing at 60°C, and 1 min of extension at 72°C. The PCR products were analyzed on a 2% agarose gel stained with ethidium bromide.

Cytokine assay

An ELISA for the detection of IFN-γ or IL-10 in plasma was conducted as described previously (16). A rat anti-mouse IFN-γ (clone R4–6A2; eBioscience) and a rat anti-mouse IL-10 (clone JES5–16E3; eBioscience) were used as the capture Abs, and a biotin-coupled rat anti-mouse IFN-γ (clone XMG1.2; eBioscience) and IL-10 (clone JES5-2A5; eBioscience) were used as the detecting Abs. The concentration of cytokines in plasma was calculated from standard curves prepared with known quantities of murine recombinant IFN-γ (Genzyme) and murine recombinant IL-10 (Pierce).

Statistical analysis

For time-series comparisons, Student's *t* test and one- and two-way ANOVAs with Fisher's PLSD post hoc test were performed using Statcel program (OMS). Survival curves were compared using a log-rank test. $p < 0.05$ was set as statistical significance of differences.

Results

Infection with Pb *XAT but not* Pb *17X induces protective immunity to* Pb *NK65*

It has been shown that mice infected with *Pb* NK65 develop severe parasitemia and die within 2 wk, although mice infected with *Pb* XAT or *Py* 17X cure spontaneously around 3 wk of infection (15, 17). To examine whether primary infection with each of the two nonlethal parasites can induce protective immunity against *Pb* NK65 lethal infection, groups of C57BL/6 (B6) mice were infected with *Pb* XAT or *Py* 17X then challenged with *Pb* NK65 on day 30 after primary infection. As expected, mice cured from *Pb* XAT infection (*Pb* XAT-immunized mice) showed extremely low levels of parasitemia after secondary infection with *Pb* NK65 (Fig. 1*A*). On the contrary, mice cured from *Py* 17X infection (*Py* 17X-immunized mice) showed high levels of parasitemia, with some delay in onset of parasitemia, and eventually died after *Pb* NK65 infection (Fig. 1*B*). These results suggest that protective immunity to *Pb* NK65 is induced by immunizing mice with *Pb* XAT but not with heterologous *Py* 17X.